

Studying the QGP with Jets at the LHC and RHIC

Leticia Cunqueiro¹ and Anne M. Sickles²

¹Laboratoire Leprince-Ringuet, Ecole Polytechnique, Palaiseau, France

²Department of Physics, University of Illinois, Urbana IL, USA

October 28, 2021

Contents

1	Introduction	2
2	A brief summary of the theoretical advances in jet quenching	3
3	Jet Measurements in Heavy Ion Collisions	5
3.1	Jet Reconstruction	5
3.2	Jet tools	7
3.3	Jet Observables	8
4	What have we learned from jet measurements at the LHC and RHIC?	11
4.1	Jet energy transport within the QGP	12
4.1.1	How opaque is the QGP to jet propagation?	12
4.1.2	How does the amount of lost energy depend on path length?	14
4.1.3	How does jet quenching depend on the characteristics of the jets?	17
4.1.4	What happens to the energy lost from jets in the QGP?	30
4.2	Effective Degrees of Freedom of the QGP	34
4.3	Critical Size for QGP Formation	35
4.3.1	Searches for Jet Quenching in pA collisions	35
4.3.2	Light ion collisions	37
5	Conclusions and Outlook	38

6 Acknowledgements	39
--------------------	----

7 References	39
--------------	----

1 Introduction

The main goal of the heavy-ion physics program at the Large Hadron Collider (LHC) and the Relativistic Heavy Ion Collider (RHIC) is to study quantum chromodynamics (QCD) at extremely high temperature. In order to do this, heavy nuclei are collided at ultrarelativistic energies. As the nuclei pass through each other, a region of extremely large energy density is created (greater than $12 \text{ GeV}/\text{fm}^3$ 1 fm after the collision [1]) and this results in the creation of matter known as the quark-gluon plasma (QGP) [2, 3, 4, 5, 6]. A major discovery of the RHIC and LHC experimental programs is that the QGP is well described as a nearly ideal fluid [7] with a maximal temperature of at least 300 MeV [8]. This strongly coupled fluid exhibits a viscosity to entropy ratio near the conjectured lower limit of $\frac{1}{4\pi}$ [9], expected for quantum fluids [10] that can be described in a dual gravity picture [11].

A key aim is to understand how such a strongly correlated liquid arises from the underlying theory, QCD, and its degrees of freedom, the quarks and gluons. Jet measurements in heavy-ion collisions are of great interest to study the microscopic structure of the QGP liquid. Since jets are multi-scale objects, they probe the QGP at varying length scales. Jets have been identified as central to understanding the nature of the interactions which give rise to the fluid-like behavior of the QGP [12, 13].

Jets in hadronic collisions are formed by the point-like scattering of quarks and/or gluons. Jets are well-defined objects in QCD and are under good theoretical and experimental control in pp collisions (see e.g Refs. [14, 15, 16]). In heavy-ion collisions, the hard, elementary scatterings leading to jet production occur in the early stages of the collision. The evolution of the scattered quark or gluon towards hadronisation is embedded with and interacts with the evolving QGP medium, and is thus subject to modifications relative to pp collisions.

The first description of the propagation of an energetic parton (quark or gluon) in the QGP appeared in Ref. [17]. Further studies identified the dominant mechanism of energy loss for high-energy partons to be gluon radiation induced by the QGP [18, 19, 20]. QGP-induced modifications to jet properties are generically called jet quenching because the most direct consequence of parton energy loss in the QGP is the reduced energy of jets, resulting in a reduced number of reconstructed hadrons and jets in heavy-ion collisions at a fixed momentum compared to expectations from pp collisions.

Jet measurements in heavy ion collisions, as we will discuss in the next sections, attempt to capture the full dynamics of jet quenching across different jet radii, collision geometry and energy. They comprise survival rates constructed as ratios of jet (or hadrons from jets) cross sections relative to expectations based on pp collisions as well as the jet radius, R , dependence of jet cross sections, inter-jet correlations, jet azimuthal anisotropies and measurements of the jet shapes, fragmentation and substructure.

Determining QGP properties from the jet modifications is not trivial. First, the precise mechanisms of jet-medium interactions are currently under investigation and the predictive power of the different theoretical formalisms and approximations are still to be validated. Second, jet measurements are often affected by multiple confounding effects. Also, any measurement of jets is necessarily made after it has propagated through the entire time evolution of the QGP and effects preceding and following the QGP existence can impact measured quantities. Finally, jet measurements in heavy-ion collisions are experimentally challenging due to the large and fluctuating background from the underlying event in a typical heavy-ion collision.

In this review, we will first discuss how jet measurements in heavy-ion collisions are performed. Then we will focus on three important questions related to the physics of jet quenching whose answers are not yet complete but will be within reach in the next few years due to new experimental data from RHIC and the LHC and theoretical advances:

- How is jet energy transported within the QGP?
- What are the effective degrees of freedom of the QGP?
- Is there a critical size for QGP formation?

We will end with a brief conclusion and outlook.

2 A brief summary of the theoretical advances in jet quenching

A highly energetic parton that propagates through high-temperature and high-density QCD matter is expected to lose energy mainly via radiative processes [18, 19, 20]. These processes consist of gluon radiation induced by the scattering of the energetic parton with the medium constituents. A radiated single gluon spectrum master formula was derived within the Baier-Dokshitzer-Mueller-Peigne-Schiff-Zakharov

(BDMPS-Z) formalism in the 1990s [20, 19, 21]. Two limiting approximations, allowing for a semi-analytical treatment of the calculations to make them numerically tractable, are traditionally considered.

- the limit where the interactions with the medium are few hard scatterings, where an expansion in terms of the number of scatterings with the medium is possible -also known as the opacity expansion, independently derived by Gyulassy-Levai-Vitev (GLV) [22].
- the limit where the interactions where there are multiple, coherent and soft interactions with the medium [23, 20, 19, 21]. In this limit, the medium-induced gluon spectrum is controlled by a single parameter, the transport coefficient \hat{q} , which quantifies the average momentum transferred from the medium to the parton per unit path length. Similar resummation of multiple scatterings are also considered in the Arnold-Moore-Yaffe (AMY) formalism [24, 25, 26] where the complete thermal propagators can be included at the price of considering only infinitely long media -this limitation was overcome in [27].

The dilute medium approximation, where only a few, normally one, scattering is considered, is also the focus of the "Higher-twist" approach in which induced gluon radiation is computed in the DIS kinematics as a higher-twist radiative correction to the inclusive cross section [28, 29].

Further important theoretical developments followed, such as the calculation of the medium-induced gluon spectra off a $q\bar{q}$ antenna [30, 31, 32, 33, 34, 35, 36, 37] which addressed color coherence in multi-gluon emissions in medium. These developments exposed a new transverse scale, the medium correlation length. This scale dictates up to which transverse distance a pair of partons remains color-coherent and thus resolved by the medium as a single color charge. The role of these interferences in the two-gluon radiation spectrum was also studied in a series of papers [38, 39, 40].

Recent theoretical work aims at increasing the precision of the analytical calculations by relaxing the approximations. The main difficulty is the correct treatment of the multiple scatterings with the medium and their interference as described by the Landau-Pomeranchuk-Migdal (LPM) effect [41]. This has been done numerically [42, 43] or at next-to-leading order (NLO) in a new expansion scheme [44], the Improved Opacity Expansion (IOE) [45]. A medium-induced gluon spectrum and further jet observables that incorporate both the soft and hard limits are essential as a theoretical reference for probing the shortest length scales in the QGP, including answering whether it is possible to resolve point-like scattering within the QGP.

In some cases, analytical calculations of jet observables are available. For instance, a first-principle calculation of the jet R dependence of inclusive jet suppres-

sion was recently presented [46], incorporating both latest NLO calculations of the gluon spectrum in the IOE and color coherence effects. The Soft Collinear effective theory SCET [47] and its extension to heavy ions, SCET_G [48, 49] have provided a framework to calculate jet cross sections and substructure [50, 51].

In order to do jet phenomenology and to compare theory expectations to jet measurements, Monte Carlo implementations are used in most of the cases since they bring in important higher-order corrections via the parton shower and the possibility to include the development of the parton shower through the lifetime of the QGP. Theoretical prescriptions for single gluon medium-induced emissions are incorporated into Monte Carlo generators [52, 53, 54, 55, 56, 57, 58].

As the jet shower develops and the jet constituents become softer and softer, the fate of such energy and the medium response to it can be described using transport models [59, 60, 61, 54]. Some models describe the medium response via recoil particles while others describe it hydrodynamically after local thermalisation (see Ref. [62] for a review).

All the above developments rely on the applicability of perturbative QCD. However jets are multiscale objects and as the partons in the shower evolve, they will reach scales that are of the order of the QGP temperature for which a weak coupling description might no longer be valid. The dual gravity picture has made possible to use holographic calculations to study energy loss in a strongly coupled QGP [63]. The Hybrid Model [64] uses a Monte Carlo approach that incorporates holographic prescriptions for energy loss.

This section is meant to briefly present the theoretical context for the jet measurements in heavy ion collisions that will be discussed in the following. We point the reader to some recent theory reviews [65, 66, 67] for further reading.

3 Jet Measurements in Heavy Ion Collisions

3.1 Jet Reconstruction

The standard jet finding algorithm used in heavy ion collisions is the anti- k_T algorithm [68] as implemented in the FastJet package [69] due to its wide adoption in the high-energy physics community, performance, and resilience to back-reaction [70]. Various constituents, underlying event subtraction and corrections for the jet energy resolution and detector effects have been used in heavy-ion measurements.

Jet measurements in heavy ion collisions have used different constituents for the jets. One approach is to only use charged particles reconstructed in the tracker as jet constituents. The advantage to this is that there is a clear connection between

the particles which make up the jet and the measured constituents. Another advantage is the excellent pointing and angular resolution of tracks, which is relevant for substructure measurements. The two main downsides are that neutral particles (one third of the jet on average) are completely excluded from track-based jets and that tracking generally becomes difficult when the track density is large (as in the core of a jet) and the particles are at high- p_T where the track momentum resolution increases. Given the potential benefits of track-based measurements in terms of precision (see for instance ATLAS jet substructure measurements in Ref. [71]), theoretical tools such as track functions [72] are being developed to analytically calculate track-based observables.

Another technique is to use purely calorimetric information, utilizing both hadronic and electromagnetic calorimetry. In this case, a much more complete picture of the jet is formed (only muons and neutrinos which carry, on average, a very small fraction of the jet energy are excluded). Additionally, calorimeter measurements improve with increasing energy (up to the point at which energy leakage becomes significant). One issue with this is that the calorimeter response can depend on the fragmentation pattern of the jet (e.g. Ref. [73]). Particle flow jets, first used in ALEPH [74], are commonly used in high-energy physics and are increasingly used in heavy-ion collisions as well. For instance, CMS uses particle flow reconstruction for jet physics both in pp and Pb+Pb [75].

Particle flow is an optimized combination of calorimeter and tracking information that is used to try to make the jet constituents closer to the actual particle constituents. This combines the advantage of track-based jets that the jet constituents are directly related to the jet particles and the advantage of calorimeter based jets that the full jet energy is measured. Additionally, particle flow facilitates pileup mitigation.

Measurements in heavy ion collision need to deal with the large level of uncorrelated underlying event background that modifies the jet p_T and the jet internal structure. On average, the underlying event shifts the jet p_T proportionally to the jet area. The underlying event fluctuations increase the jet energy resolutions more strongly for increasing R .

The correction procedure is in general characterized by:

- An event-by-event correction of pedestal background that affects the jet p_T and its substructure
- A suppression of combinatorial (fake) jets, which are the jets that are reconstructed by the algorithm but are not correlated to a hard scattering. Similarly, combinatorial contributions to the jet substructure are suppressed.

- The unfolding of detector effects and residual background fluctuations

The first step requires an estimate of the average uncorrelated background per unit area, $\rho(\eta, \phi)$. A common procedure is the area-based method [76]. An extension of the area-based method to correct jet shapes or any IRC-safe substructure observable for the average background is also applied by the different experiments [77]. ATLAS has used an iterative determination of $\rho(\eta, \phi)$ based on the region of the detector which doesn't have candidate jets [78]. Other approaches, that consider a particle-by-particle subtraction are also used, see for instance [79, 80].

The impact of combinatorial jets is mitigated when considering high- p_T jets and/or small jet radius, R . For low- p_T jets and/or large R different techniques have been applied like a data-driven subtraction procedure based on semi-inclusive coincidences (recoil) [81], requirements on the jet structure [82], event mixing [83] or machine-learning (ML) [84].

When measuring jet substructure, the problem of combinatorial subjet prongs emerges. When selecting two subjet prongs, for instance via the SoftDrop (SD) grooming procedure [85], the purity of the measured prongs is not unity [86], and it decreases with lowering z_{cut} , grooming cuts or increasing jet R . To assess this problem, the strategy in recent measurements was to consider small- R jets and high z_{cut} grooming cuts. There is room to improve this substantially in the near future.

The last step is the unfolding. The Bayesian [87], SVD [88] or TUnfold [89] algorithms are common unfolding tools used by the different collaborations to correct detector and residual background fluctuations in one or several dimensions. New tools based on ML are currently used to correct for detector effects in the context of high energy physics [90] and are yet to be explored in heavy-ion collisions. In some cases the measurements are not unfolded to the particle level and theoretical calculations are smeared to match the data. However, this approach prevents direct comparisons between results of different measurements.

3.2 Jet tools

In recent years, the application of theoretical and experimental jet tools developed by the high-energy physics (HEP) community to heavy-ion collisions has opened new opportunities, particularly in the area of jet substructure. In HEP, jet substructure has a broad set of applications, from tagging massive boosted particles or tuning MC generators, to testing the standard model or enhancing sensitivity to new physics [16]. Jet substructure can be studied using the clustering history. The jet constituents are typically reclustered with the Cambridge/Aachen (CA) algorithm [91, 92], which combines pairs of constituents/subjet prongs with the smallest angular separation

first, leading to an angular-ordered jet tree. Then the clustering history can be undone. Each step of the declustering yields two subjets $S1$ and $S2$ with transverse momenta $p_{T,1}$, $p_{T,2}$ separated by a distance $\Delta R_{12} = \sqrt{\Delta y_{12}^2 + \Delta \phi_{12}^2}$ and with $p_{T,1} > p_{T,2}$. The process can be iterated always unclustering the leading prong $S1$ until two subjet prongs are found that satisfy a given kinematic condition—this is what grooming algorithms do as we will describe. Or the process can be iterated till the given $S1$ cannot be unclustered (when it is a single-particle prong), to study the kinematics of all the jet prongs and build what is called the primary Lund Jet Plane [93].

The massDrop/SoftDrop groomer [94, 85] stops the declustering when the following conditions are met:

$$z_{12} = \min(p_{T,1}, p_{T,2}) / (p_{T,1} + p_{T,2}) > z_{cut} (\Delta R_{12} / R)^\beta \quad (1)$$

where β and z_{cut} control the grooming and are choices in a particular analysis. In essence, the algorithm removes large-angle and soft branches until a sufficiently hard splitting is found. The resulting groomed jet is less affected by non-perturbative effects like the underlying event or pileup. Another recently developed grooming algorithm is the dynamical groomer [95].

Alternatively, instead of using the clustering history to select hard substructure, jet trimming [96] consists of reclustering the jet constituents with a resolution parameter smaller than the original jet R to keep only the subjets that satisfy $p_{T,sub} > z_{cut} p_{T,jet}$. Those subjets which kept are merged to form the trimmed jet.

In heavy-ion collisions, the possibility to select hard components of the parton shower to study microscopic properties of the QGP has generated a lot of theoretical and experimental interest and new synergies between the HEP and HI communities.

3.3 Jet Observables

In order to capture the physics of jet quenching, three different classes of observables are studied:

- inclusive jet suppression
- inter-jet correlations via hadron-jet, boson-jet or di-jet coincidence measurements.
- intra-jet distributions, via jet shapes and jet substructure

These classes of observables are sensitive to different aspects of jet-medium interactions and must be dynamically correlated. Here we define several of the common quantities used in this field.

Inclusive jet suppression The first class of observables are simply yield measurements of single jets (or hadrons). These yield are compared to expectations from scaling cross sections in pp collisions $\frac{d^2\sigma_{jet}}{dp_T dy}$ by the nuclear thickness function, $\langle T_{AA} \rangle$. This is quantified by the nuclear modification factor

$$R_{AA} \equiv \frac{\frac{1}{N_{evt}} \frac{d^2 N_{jet}}{dp_T dy}}{\langle T_{AA} \rangle \frac{d^2 \sigma_{jet}}{dp_T dy}}. \quad (2)$$

For objects which lose energy traversing the QGP, R_{AA} is less than unity but the value of R_{AA} depends on the amount of energy lost by the jet and the shape of the underlying p_T spectrum of the objects of interest. For a fixed energy loss, a spectra with a steeper p_T dependence will have a smaller R_{AA} value. In the absence of a pp reference dataset, R_{CP} , the central to peripheral collision yield ratio, has been measured:

$$R_{CP} \equiv \frac{\langle T_{AA} \rangle_{per} \frac{1}{N_{evt,per}} \frac{d^2 N_{jet,cent}}{dp_T dy}}{\langle T_{AA} \rangle_{cent} \frac{1}{N_{evt,cent}} \frac{d^2 N_{jet,per}}{dp_T dy}}, \quad (3)$$

where $\langle T_{AA} \rangle_{cent}$ and $\langle T_{AA} \rangle_{per}$ are the nuclear thickness function for the central and peripheral events, respectively. In all cases $\langle T_{AA} \rangle$ is calculated via the Glauber model [97].

In addition to the absolute rate of jet production, the the azimuthal variation of the jet yield relative to the event plane angles can be measured. This is quantified via the vn coefficient defined as: [7]:

$$\frac{dN}{d\phi} \propto 1 + 2 \sum_{n=1}^n v_n \cos(n(\phi - \Psi_n)) \quad (4)$$

Since the event planes are understood to be driven by the geometry of the overlap of the two nuclei in the collision, jet- v_n measurements are sensitive to the dependence of energy loss on the length of the QGP seen by the jet.

Inter-jet correlations This class of measurements study the momentum balance and the azimuthal correlation between a jet and another object. These observables exploit the fact that high- p_T objects must be produced in momentum conserving processes and that these are dominantly $2 \rightarrow 2$ scatterings. A common example is where one object is a high- p_T photon and one is a jet. The photon doesn't interact strongly with the QGP and thus retains its original momentum. The jet is produced

opposite in azimuth and its momentum and direction can be changed by interacting with the QGP. The momentum balance is quantified via:

$$x_{J\gamma} \equiv \frac{p_T^{\text{jet}}}{p_T^\gamma}. \quad (5)$$

Because the photon momentum is unaltered, differences in this quantity between heavy-ion collisions and pp collisions are attributable to energy loss.

The same technique can be used when both of the objects are jets. In that case the quantity:

$$x_J \equiv \frac{p_T^{\text{jet,subleading}}}{p_T^{\text{jet,leading}}} \quad (6)$$

is measured. Here the labels *leading* and *subleading* denote the highest and second highest p_T jets in the event, respectively. The interpretation isn't as simple as in the photon-jet case because the leading jet can also lose energy, however this observable is sensitive to the difference in energy loss between the leading and sub-leading jets.

Intra-jet observables The intra-jet observables measured in heavy ion collisions can be further classified into:

- Those that are built directly from the positions and momenta of the jet constituents. Examples of this are jet fragmentation functions, which provide information on how jet constituents carry the jet momentum, or what are called generalised angularities, a set of observables that can be constructed as moments of the angle of the constituents relative to the jet axis and the constituent energy. Examples of measured angularities are the jet mass, the jet girth, g , and the momentum dispersion, $p_{T,D}$.
- Those that are built using the jet clustering history. The re(de)clustering process introduces a hierarchy and is used to access parts of the jet tree that are well defined theoretically and that are expected to be connected to the gluon emissions in the parton shower process. Examples of such observables that will be discussed in this review are the groomed momentum balance z_g , the groomed jet radius R_g , the Les Houches multiplicity n_{SD} , the N -subjettiness or the k_T distance.

Fragmentation functions are typically measured as a function of:

$$z \equiv \frac{p_T^{\text{part}} \cos \Delta R}{p_T^{\text{jet}}} \quad (7)$$

where p_T^{part} is the transverse momentum of the particle of interest, ΔR is the angular distance between the jet axis and the particle and p_T^{jet} is the transverse momentum of the jet. In this way, z represents the longitudinal momentum fraction of the particle with respect to the jet. Other definitions of fragmentation functions, including as a function of p_T^{part} and in two dimensions, both angular and longitudinal directions, have been considered.

The angularities can be described as a two-parameter family of observables [98]:

$$\lambda_{\beta k} = \sum_{i \in \text{jet}} z_i^k (R_i/R_0)^\beta \quad (8)$$

where the particular choice of parameters $(\beta, k) = (0, 0), (0, 2), (1, 1), (2, 1)$ correspond to jet multiplicity, $p_{T,D}$, girth and jet mass respectively.

Different observables belong to the second category that uses the clustering history will be described as discussed in the following sections.

4 What have we learned from jet measurements at the LHC and RHIC?

We have organised available heavy-ion jet data around three physics questions. First, what are the mechanisms responsible for the transport of energy from high-energy to low-energy modes within the QGP? Second, can we observe jets probing free quarks and gluons within the QGP? And finally, what is the critical size for the QGP formation? The first class of measurements constrains the mechanisms of jet-medium interactions since it comprises a vast set of observables that are differential in jet size, flavour, shape, substructure and in-medium path length. We reconstruct jets after they interacted with the QGP and we measure the properties of a specific selection of jets, those which have survived. We aim to learn about flavour hierarchy in energy loss, about the role of the medium response, or the interplay between energy loss and color coherence. These aspects of jet quenching are interconnected and measurements attempt to isolate the effects, for instance, by separating large-angle and small-angle components or by selecting jets with a hard 2-prong substructure. The second class of observables comprise searches of large momentum transfer interactions in the medium as a proof of point-like scatterers within the QGP fluid. The third class of measurements comprises searches for jet quenching signatures in small systems like p +Pb collisions that display signatures of collective effects.

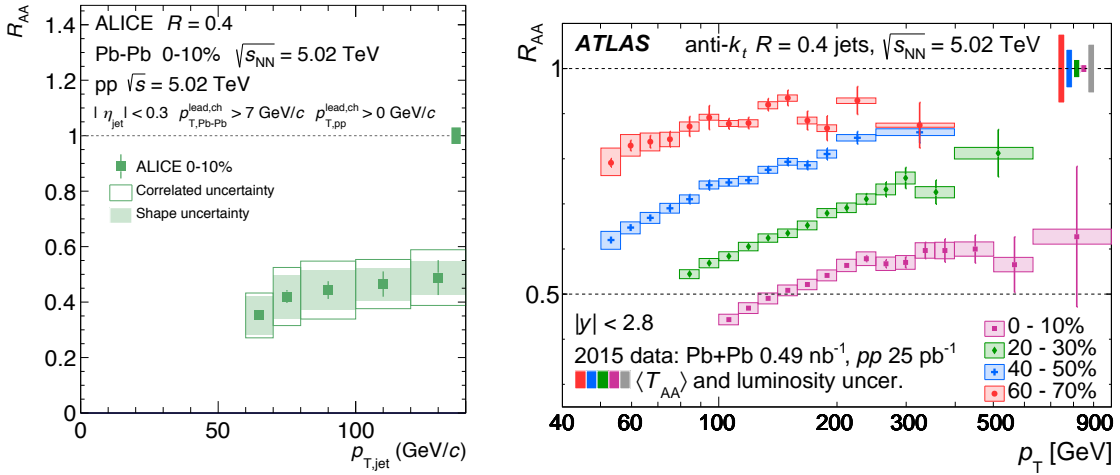


Figure 1: Jet R_{AA} as a function of p_T^{jet} in Pb+Pb collisions. Figures are from Refs. [99] (left) and [100] (right).

4.1 Jet energy transport within the QGP

In this section we have grouped experimental measurements into four categories according to the aspect of the jet-medium interaction mechanisms they constrain:

- How opaque is the QGP to jet propagation?
- How does the amount of lost energy depend on path length?
- How does jet quenching depend on the characteristics of the jets?
- What happens to the energy lost from jets in the QGP?

4.1.1 How opaque is the QGP to jet propagation?

Inclusive jets dominantly originate from light quarks and gluons. The high rates of these jets allow for measurements over a very large kinematic range. Figure 1 shows recent ALICE and ATLAS results of the jet nuclear modification factor, R_{AA} , measured in 0–10% central collisions from 60 GeV to 1 TeV for $R = 0.4$ jets [99, 100] for 5.02 TeV Pb+Pb collisions at the LHC. R_{AA} remains below unity over the entire measured kinematic range. At RHIC, the jet R_{CP} was measured [101] and been found to be consistent with values from Ref. [102] in 2.76 TeV Pb+Pb collisions, see Figure 2. Additionally, R_{AA} has been measured for neutral pions [103].

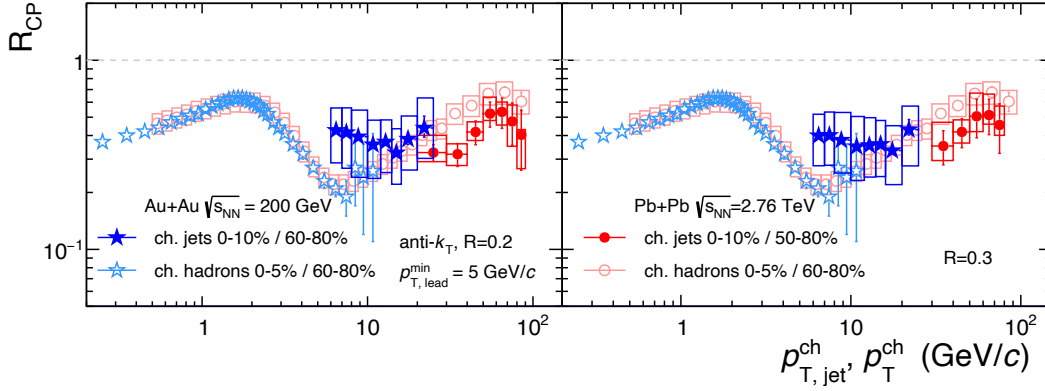


Figure 2: R_{CP} for jets and charged particles at RHIC and the LHC (as indicated on the plot) for $R = 0.2$ (left) and $R = 0.3$ jets (right). From Ref. [101].

In order to extract energy loss values from these measurements, it is necessary to have a model. Jet quenching models are reviewed in Refs. [65, 66, 62]. A great deal of theoretical work has gone into the development of these models over many years. However, constraining models with data has been a challenge. The use of Bayesian techniques to extract jet quenching parameters is a recent but rapidly evolving field. This was first used in heavy ion collisions to constrain the equation of state [104] and is now used to extract estimates for the QGP bulk properties including shear and bulk viscosity (see recent examples in Refs. [105, 106, 107]).

From the LHC data, Ref. [108] calculated that jets have lost an average of 10–50 GeV for p_T^{jet} between 100 and 900 GeV. These energy loss values provide additional information based on the R_{AA} values, but they are not direct properties of the QGP. The extraction of \hat{q} from energy loss measurements was recently performed in Refs. [109, 110] using the LIDO and JETSCAPE software, respectively. Both of these papers constrain the models to experimental data by evolving a jet quenching calculation through a 2+1D hydrodynamic evolution (using event-averaged initial conditions). At high temperature, the two \hat{q} extractions agree and constrain \hat{q}/T^3 to be approximately 1–5 over the range $300 < T < 500$ MeV but the result from LIDO increases sharply to 10–15 for $T < 300$ MeV, while the result from JETSCAPE remains constant in that same range (both of these extractions are for $p = 100$ GeV). The extractions use different energy loss models and a different selection of experimental data and it is not clear which (or both) aspect of the models leads to the low- T difference in \hat{q} . Both extractions include data from RHIC, but LIDO includes the STAR jet R_{CP} result [101] and the PHENIX π^0 result [111] while JETSCAPE

only includes the PHENIX π^0 result. JETSCAPE has broken down the constraints on \hat{q} from RHIC and the LHC data separately and shown that there is essentially no constraining power in the RHIC data in their model due to the limited kinematic range of the measurement. The limited kinematic range and statistical precision of the available RHIC data mean that the extractions are dominated by the LHC data at 5.02 TeV. This should change with data from the sPHENIX experiment [112].

The ability to extract \hat{q} from the data via Bayesian analysis is a substantial step forward in jet physics in heavy ion collisions. The current analyses represent a proof of concept of the Bayesian techniques and are improvable in several ways. On the one hand, next generation of analysis will include more differential jet observables that pose more constrain to the models than single hadron or fixed- R inclusive jet suppression. On the other hand, a wider set of model calculations and approximations should be included in the analysis. Other aspects, like going beyond event-averaged geometry to be sensitive to geometrical fluctuations in energy loss are also to be addressed.

For the rest of this section, we discuss other measurements which can provide more experimental information about the details of energy transport in the QGP.

4.1.2 How does the amount of lost energy depend on path length?

A fundamental question is how energy loss of jets depends on the path length the jet travels through the QGP. We cannot know the specific path length traveled by the jet because of:

- event-by-event variation of the QGP shape and size
- the unknown position of the hard scattering process within the QGP
- the random propagation direction of the jet within the QGP

Because of these there can be a large variation between the path lengths encountered even by jets produced within the same hard scattering. This variation, along with the steeply falling jet cross section with transverse momentum leads to a selection bias toward jets which have lost little energy and thus likely also travelled through a smaller than average amount of QGP. This is called the *surface bias* [113].

In addition to path-length variation there can also be fluctuations in the energy loss process [114]. In order to isolate effects which are sensitive to path-length variations, jet observables which are differential in the QGP geometry can be measured. Additionally, model calculations must incorporate realistic event-by-event geometry into calculations in order to make meaningful comparisons to data. In this section,

we will discuss the physics processes thought to govern this question and the available measurements. We will finish with some open questions.

In the perturbative description of energy loss, the spectrum of the emitted gluons is expected to be $dI/d\omega \propto 1/\omega$ if the interactions with the medium are incoherent. However the Landau–Pomeranchuk–Migdal (LPM) effect in the QGP [19, 115] leads to $dI/d\omega \propto 1/\omega^{3/2}$ for $\omega < \omega_c$ and this leads to a quadratic dependence of the energy loss on the in-medium path length, L , $\Delta E_{loss} \propto L^2$. In a nonperturbative strong coupling model $\Delta E_{loss} \propto L^3$ is expected [116].

$\Delta E_{loss}(L)$ itself is not directly measurable. Instead, the key element in this study has been to measure the azimuthal anisotropy, v_n , of jets and high- p_T particles. Measurements from RHIC using hadrons showed a larger v_2 than expected from pQCD-based energy loss calculations [117]. This was taken as possible evidence for strong coupling energy loss with a stronger dependence on L than expected from pQCD. However, conclusions made from these measurements were shown to be limited by the use of non-fluctuating geometry; the addition of geometrical fluctuations increased the value of v_2 expected from pQCD-based theoretical calculations [118]. At the LHC, measurements of jet [119, 120, 121] and high- p_T charged particle [122] v_2 have been performed at the LHC; a compilation of the measurements for mid-central Pb+Pb collisions is shown in Figure 3. The v_2 value varies from approximately 5% for 20 GeV charged particles to about 2% for 200 GeV jets. The v_2 values as a function of centrality follow the geometrical expectations; a smaller v_2 value is seen in central collisions than in mid-central and peripheral collisions [121]. In order to further constrain the path-length dependence of energy loss, measurements of v_3 and v_4 have been made for jets [121] and high- p_T charged particles [122]; above 20 GeV, there is no evidence for non-zero v_3 or v_4 in any collision system. These higher-order harmonics should introduce a smaller path length difference between in-plane and out-of-plane directions than v_2 and so it is important to improve the precision of these measurements in order experimentally constrain the path length dependence of energy loss.

Interestingly, a non-zero v_2 has been measured for high- p_T charged particles in p +Pb collisions [123]. The measured v_2 is approximately 2% for 20–50 GeV particles in central p +Pb collisions. In contrast to Pb+Pb collisions, the v_2 in p +Pb collisions is not accompanied by a large energy loss; in p +Pb collisions R_{pPb} is consistent with unity [124, 125]. If this v_2 arises from path-length dependent energy loss, the absolute size of the energy loss would have to be sufficiently small to accommodate the R_{pPb} results. Thus far, there is no understanding of whether the observed v_2 can be attributed to energy loss or if some other source is required to explain the data. If the p +Pb v_2 is due to some other mechanism than path-length-dependent energy loss,

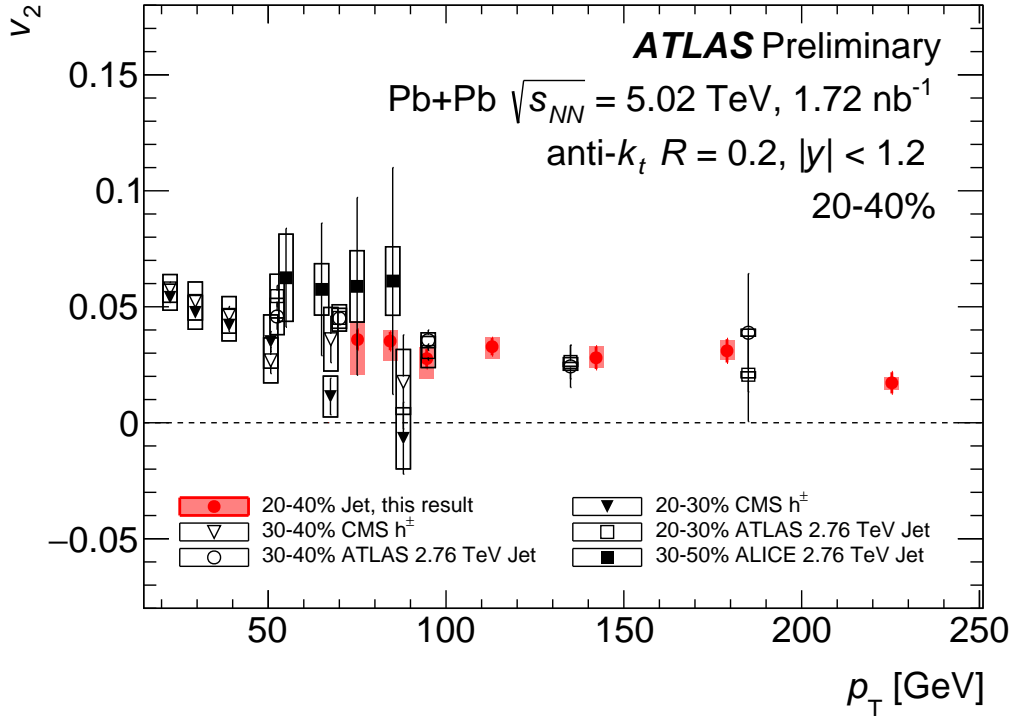


Figure 3: A compilation of jet [120, 121] and charged-particle [122] v_2 measurements. Figure is from Ref. [121].

then the impact to the commonly accepted understanding of these measurements in heavy-ion collisions needs to be assessed.

Dijet measurements provide a different sensitivity to the path-length dependence of energy loss through geometry than single-jet measurements. The first LHC results showed a significant depletion of balanced dijets in Pb+Pb collisions [126]. The qualitative explanation for this is that one jet loses more energy than the other, either through an asymmetry in the path length or through fluctuations in the energy loss. Current measurements show the same decrease in the fraction of balanced jet pairs in central Pb+Pb collisions compared to pp collisions, up to leading jets of at least 400 GeV [127] (see Figure 4). For leading jet p_T of 158–178 GeV the x_J distribution in central Pb+Pb collisions is consistent with no x_J dependence over the range of $0.5 < x_J < 1.0$. This is a very broad distribution and suggests that there is a very wide variation in the magnitude of energy loss experienced by the subleading jet in these collisions. At 2.76 TeV, the first unfolded dijet measurements in Pb+Pb

collisions also showed the imbalanced pairs expected from energy loss, but also an apparent peak in the x_J distribution at approximately 0.5 [128]. Figure 4 shows the x_J distributions (after the unfolding) in central Pb+Pb collisions for jets from 100 GeV to over 200 GeV. The peak structure is clear for the lowest p_T jets and becomes insignificant for $p_T > 126$ GeV. The origin of this structure is not known. New measurements at 5.02 TeV have been unable to reach as low in jet p_T to confirm this structure [127].

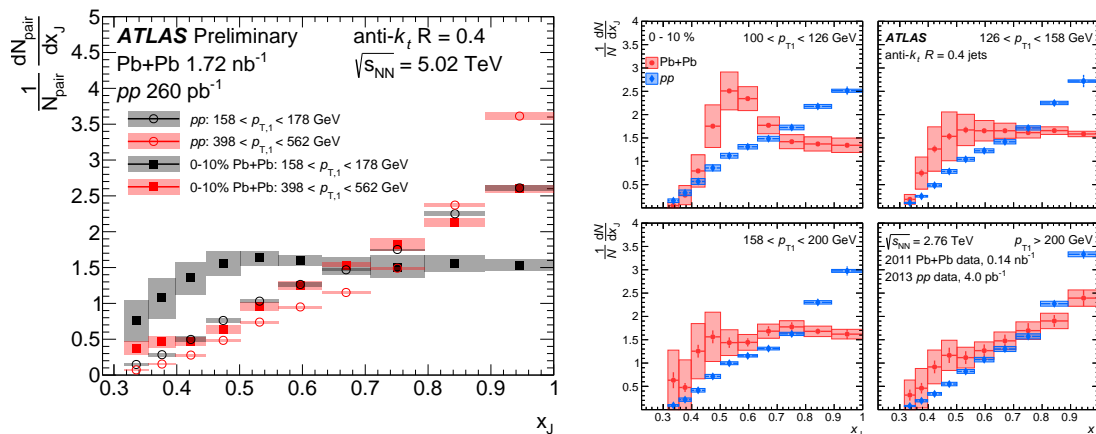


Figure 4: Dijet momentum imbalance, x_J , at 5.02 TeV (left) and 2.76 TeV (right) for 0–10% central Pb+Pb collisions and pp collisions. Figures are from Ref. [127] (left) and Ref. [128] (right).

Both the dijet imbalance and the jet azimuthal anisotropies should be especially sensitive to the effects of fluctuations in the initial geometry and fluctuations in the energy loss process. Due to this it is important to simultaneously experimentally constrain these quantities and compare them with theoretical calculations.

4.1.3 How does jet quenching depend on the characteristics of the jets?

In the previous sections, jets were discussed as monolithic objects. Here, we discuss measurements of the jet properties that were done in order to probe the medium-modifications of the internal jet radiation pattern. Such modifications can provide information on the microscopic details of the jet-QGP interactions.

The jet radiation pattern is explored via measurements of the jet shapes including fragmentation functions. We also discuss varying the *partonic flavor* of jets between quarks, gluons and heavy quarks, to test the flavour and mass dependence of jet-

medium interactions. Finally, we discuss measurements of the hard jet substructure which aim at probing the building blocks of the parton shower in medium.

Does jet quenching depend on the jet shape or are harder narrower jets quenched less?

Differences in the parton shower evolution are expected to lead to different energy loss, so it is reasonable to ask if the structure of the jets which survive is modified from jets in pp collisions. This question is intrinsically related to the quark/gluon differences discussed in the next subsection because gluon jets on average have a broader and softer fragmentation than quark jets.

The most comprehensive measurement of jet fragmentation in heavy-ion collisions is in Ref. [129]. Figure 5 shows the fragmentation functions in central Pb+Pb events for $R = 0.4$ jets divided by the same quantity in pp collisions for three jet p_T selections. The momentum fraction of the jet carried by the charged particle, z , is determined with respect to the *observed* jet energy (as opposed to the original, pre-quenching, parton energy). At high- z the ratios of the fragmentation functions are consistent for all three jet p_T selections and there is an excess of high- z particles in Pb+Pb collisions. This excess can be explained as the result of a selection bias: the measured jets with high- z hadrons are jets with a harder fragmentation that have been quenched less. Since quark jets have harder fragmentation on average than gluon jets, this could also be understood as evidence for a stronger energy loss for gluon jets than quark jets [130] resulting on an enhanced quark fraction at given p_T^{jet} .

In order to look at the angular distribution of energy in jets, jet angularities and other jet shapes have been measured [131, 132]. The measurement in Ref. [131] measures the distribution of calorimeter energy inside the jets. Ref. [132] is based on unfolded $R = 0.2$ track-based jets and includes $p_T^{\text{part}} > 0.15$ GeV and measures both the angularity, g and the momentum dispersion $p_T D$. These observables correspond to $\lambda_{0,2}$ and $\lambda_{1,1}$ in Equation 8 respectively. The small cone size of these jets emphasizes the core and minimizes the effect of any medium response. The distributions of these quantities in Pb+Pb collisions are shown in Figure 6 and indicate that the measured quenched jets are narrower and have a harder fragmentation than the PYTHIA [133] simulation of jets in the vacuum. This can, yet again, be interpreted as a selection bias by which broad jets with a softer fragmentation are more quenched and are filtered out from the selected reconstructed jet p_T bin. Interestingly, like in the fragmentation function measurements from ATLAS above, a harder and narrower fragmentation is consistent with a more quark-like fragmentation and the results agree well with PYTHIA quark distributions as shown in [132]. It is however worth noting that the measurement of the jet charge [134] does not indicate a

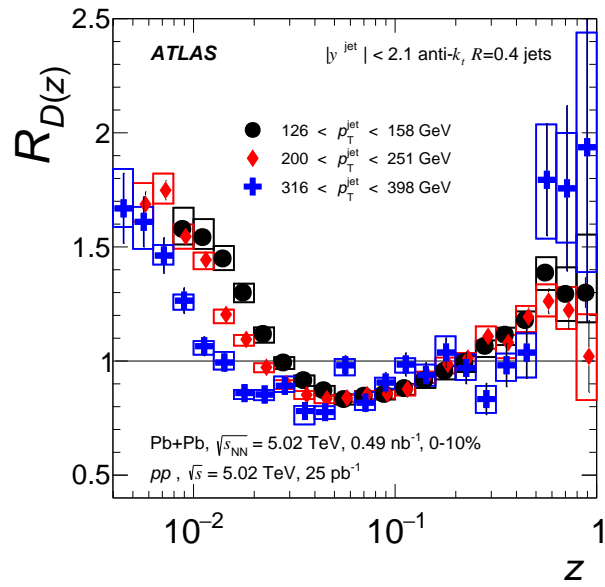


Figure 5: Ratios of the fragmentation functions in central Pb+Pb collisions to those in pp collisions for three different p_T^{jet} selections as a function of z . Figure is from Ref. [129].

change of quark and gluon fractions in Pb+Pb relative to pp collisions.

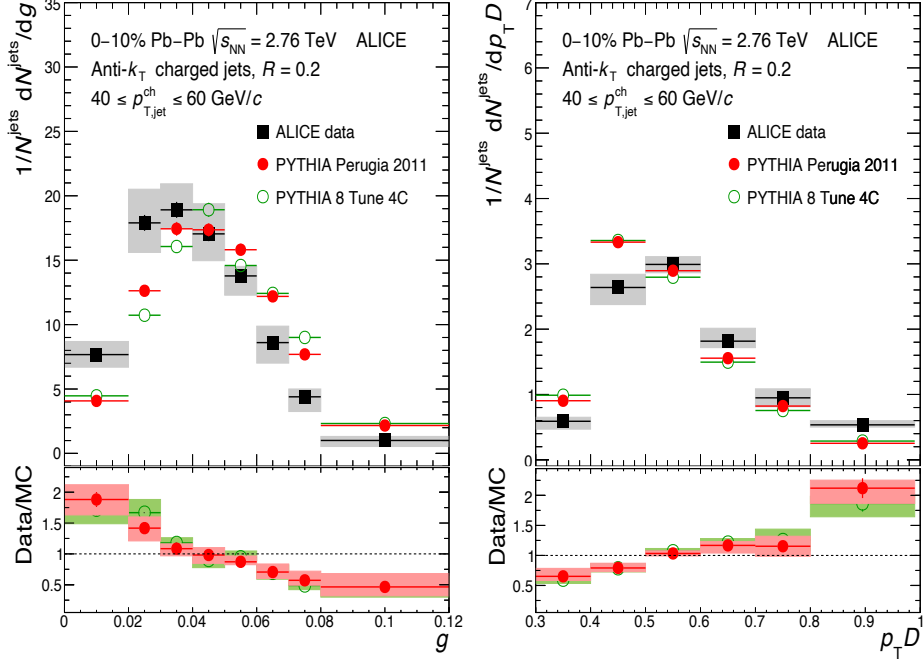


Figure 6: Jet girth and momentum dispersion in central Pb-Pb collisions compared to a vacuum simulation, from Ref. [132].

Does jet quenching depend on quark flavour and mass?

At leading order in vacuum QCD, differences between quark and gluon fragmentation are dictated by color factors: the splitting rate is enhanced by the color factor and is 2.25 times higher for gluons than for quarks, leading to broader and softer parton showers. The larger splitting rate leads to an expectation of more interactions between gluon jets and the QGP.

Inclusive jets are mixture of quark and gluon jets. The mixture is governed by the parton distributions functions (PDFs) of the colliding nucleons. At low- x , gluons dominate and toward the valence region there is a greater fraction of quarks. An attempt to measure the quark and gluon fractions in jets in Pb+Pb collisions has not found any significant difference from that measured in pp collisions [135], but such measurements have substantial systematic uncertainties and model dependence. Other techniques have been used to attempt to enhance the quark-jet fraction and to look at the effect on the jet quenching. One technique to enhance the quark-jet sample is to measure the rapidity dependence of jet observables. At forward rapidities,

the fraction of quark initiated jets will be enhanced because the jet partons come from higher- x partons than at smaller rapidities. Alternatively, one can consider jets recoiling from isolated photons or Z-bosons. PYTHIA simulations [136] indicate quark fractions nearly a factor three higher in Z-jet events than in central dijet events for $R = 0.4$ jets of $p_T < 200$ GeV at 13 TeV. Lastly, heavy flavour jet tagging allows to study the effect of large quark mass on jet quenching.

- Rapidity dependence of energy loss Figure 7 shows the first evidence for a rapidity dependence of R_{AA} [100]. There are two competing effects that could be expected. First, the gluon jet fraction in the inclusive jet sample decreases toward increasing rapidity at fixed jet transverse momentum, p_T^{jet} , (see, for example Ref. [130] where the PYTHIA8 calculations show that the quark fraction almost doubles at forward rapidities $1.2 < |y| < 2.1$ compared to $|y| < 0.3$ for jets of $p_T = 100$ GeV.) As quarks are expected to lose less energy than gluons in the QGP, the value of R_{AA} would be expected to increase as $|y^{\text{jet}}|$, and thus the fraction of quark jets in the inclusive jet sample at a fixed p_T^{jet} , increases. Second, the p_T^{jet} spectra become steeper with increasing $|y^{\text{jet}}|$ (see, for example Ref. [137]); this would cause a reduction in the R_{AA} value for the same energy loss. Figure 7, R_{AA} is shown to decrease with increasing $|y^{\text{jet}}|$ for jets with $p_T^{\text{jet}} > 300$ GeV, suggesting that the second effect dominates for these jets.
- Photon-tagged jet observables

Jets opposite in azimuth from a high momentum photon can also provide an enhancement of quark-jets over inclusive jets because these photon-jet pairs are primarily produced via $g + q \rightarrow \gamma + q$ scattering. Additionally, the photon does not lose energy in the QGP via the strong interaction and therefore provides information about the initial hard scattering momentum transfer. However, these jets have a different geometrical bias than inclusive jets; since the photon does not lose energy, the geometrical bias toward jets produced near the surface is removed for photon-jet measurements.

Previous measurements have shown the p_T of the jet relative to that of the photon is reduced in heavy-ion collisions relative to pp collisions [138]. Measurements allow the study of the photon-jet momentum balance as a function of the photon p_T [139, 140]. The ATLAS results are unfolded and are shown in Figure 8 for 100-158 GeV photons in 0–10% central collisions. Going from peripheral to central collisions, the fraction of balanced photon-jet pairs (those with $x_{J\gamma} \approx 1$) decreases and the fraction of pairs in which the photon has more p_T than the jet increases. This is qualitatively as expected from jet quenching,

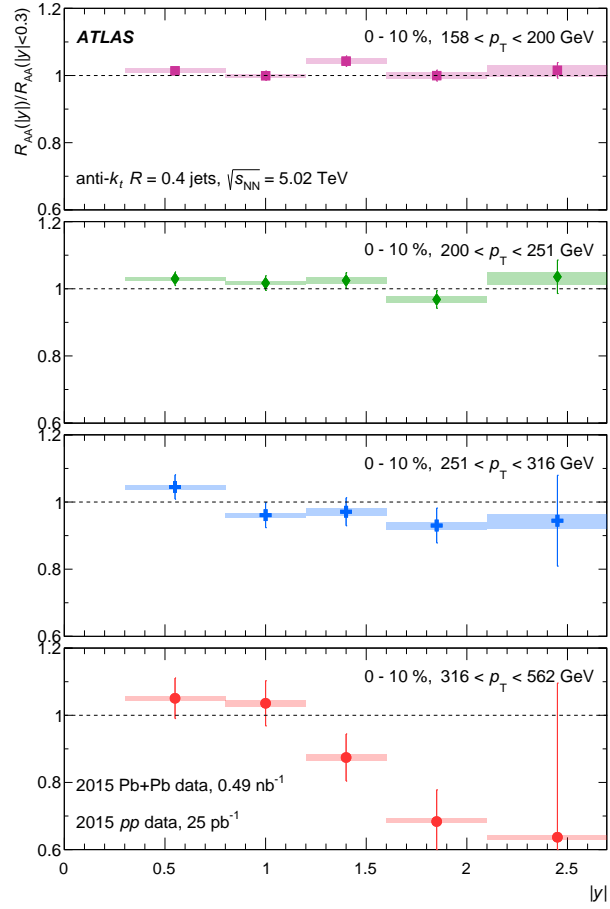


Figure 7: R_{AA} as a function of the jet rapidity normalized by $R_{AA}(|y| < 0.3)$ for four p_T^{jet} selections. Figure is from Refs. [100].

but due to the different geometrical bias and observable than the inclusive jets it is not possible to say without a model if these quark-enhanced jets have lost less energy, as would be expected. The most probable value of $x_{J\gamma}$ in the most central collisions is about 0.3, indicating that many jets have lost a large fraction of their transverse momentum. However, it is interesting that even in the most central collisions, there remain a substantial fraction of jets which are nearly balanced—indicating that they have not lost a large amount of energy. Measurements with Z -bosons as the tag have also been done [141]; the message is similar to that of the photon-tagged measurements but the statistical precision is worse.

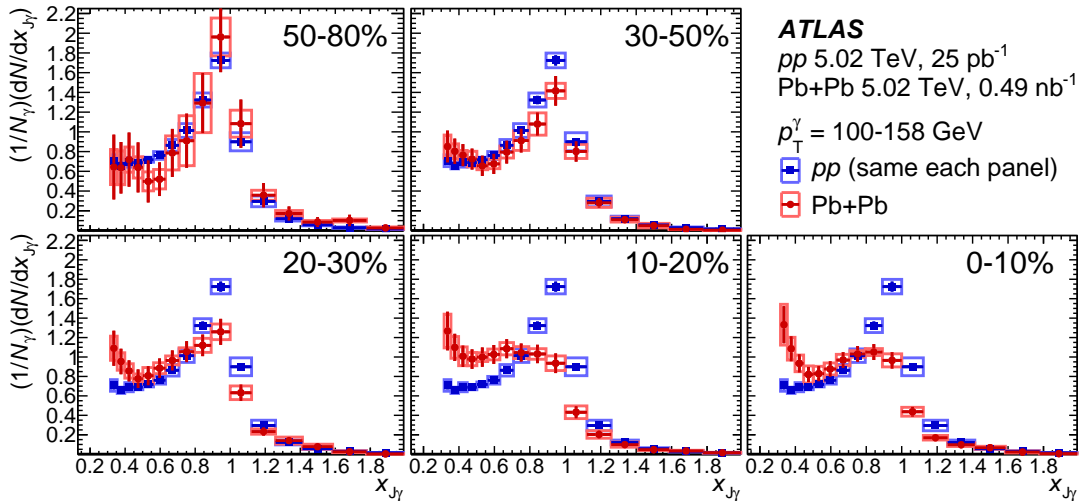


Figure 8: Ratio of the jet transverse momentum to the photon p_T , $x_{J\gamma}$, in pp and $Pb+Pb$ collisions [140].

First measurements of the fragmentation of the jets opposite a photon have been performed [142, 143]. As discussed above, these fragmentation functions differ from inclusive fragmentation functions in a few ways. First, the jets are possibly quenched more due to geometrical bias from the photon selection. Second, the jets are at lower p_T^{jet} than the inclusive jet fragmentation functions because the tagging with the photon limits the statistics and provides a cleaner identification of jets at lower p_T^{jet} than in the inclusive case. Finally, these jets have a much higher fraction of quark jets than the inclusive jet sample do to the leading order dominance of the $q + g \rightarrow q + \gamma$ process in these events. Measurements of photon-hadron correlations had been made at RHIC [144, 145, 146], but only recently were measurements made of the hadrons in reconstructed jets

back-to-back with a photon in Pb+Pb collisions [142, 143]. Figure 9 shows the ratio fragmentation functions in Pb+Pb collisions compared to pp collisions for both jets opposite a photon and inclusive jets. A stronger deviation of this ratio from unity is seen in central collisions than in peripheral collisions for both jet selections. Interestingly, when comparing the central data directly to the peripheral data, the centrality dependence is significantly larger in the photon-tagged jets than in the inclusive jets. It is not known if this is caused by the lower p_T^{jet} range for the photon-tagged fragmentation functions or the different geometrical biases of the two samples, but being able to measure the fragmentation of photon-tagged jets at the same p_T^{jet} as inclusive jets would be an obvious way to constrain the source of this difference.

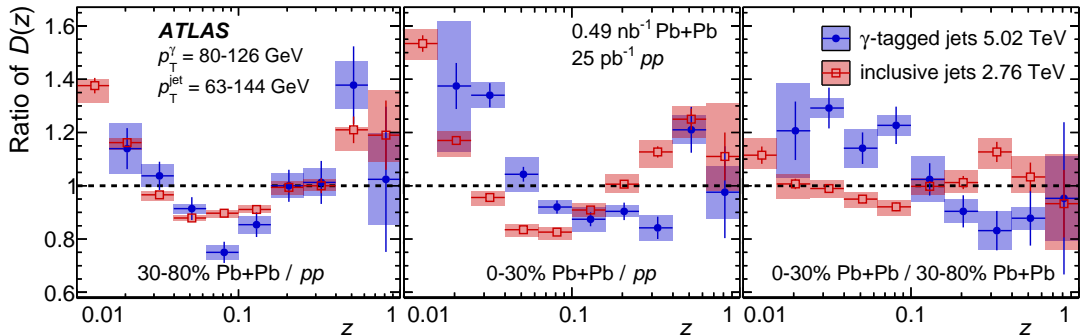


Figure 9: The ratio of the fragmentation function as a function of charged particle p_T in central Pb+Pb collisions to pp collisions for jets opposite a photon (squares) and inclusive jet fragmentation functions [147] (circles). Figure is from Ref. [143].

- Heavy Flavour

In vacuum, besides the aforementioned differences between the radiation pattern of jets initiated by light quarks and gluons, dictated at LO by the color factors, quark mass plays a role. In QCD (and in gauge theories in general), radiation off a massive quark Q is suppressed in a cone of angle $\theta_C = m_Q/E_Q$. This is the so-called dead cone effect [148] that causes heavy quarks to radiate less than light quarks. In heavy ion collisions, medium-induced radiation off heavy quarks is expected to fill the dead-cone region, but is predicted to be suppressed for high energy radiation as compared to light quarks [149] resulting on a quark mass-dependence to energy loss.

The measurement of energy loss of heavy flavor jets is very challenging. The overall rate of these jets is very low (a few percent of the inclusive jet cross

section) and identifying them relies on measurements sensitive to the decay of the B or D hadron carrying the quark of interest inside the jet. CMS has made a measurement of the b -jet R_{AA} in 2.76 TeV collisions [150] and found consistent R_{AA} values between inclusive and b -jets. Additionally, they measured the momentum imbalance of back-to-back b -jets and found them to be comparable to those measured for inclusive jets in 5.02 TeV Pb+Pb collisions [151], see Figure 10. Both measurements have sizeable uncertainties and b -jet measurements will be an important part of the LHC physics program in Run 3 and beyond.

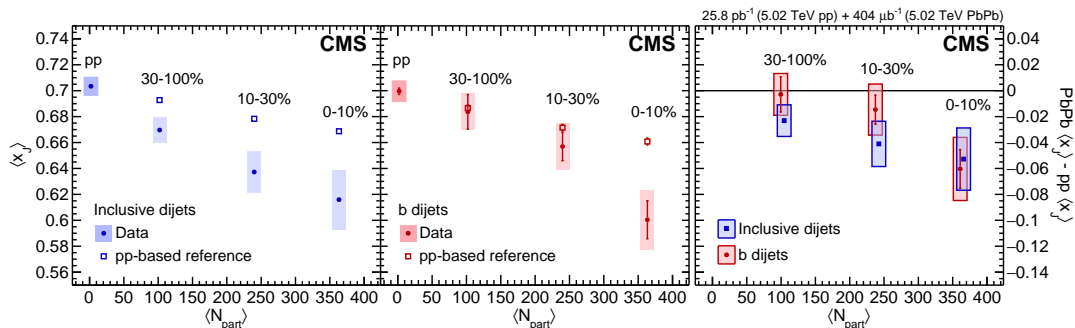


Figure 10: The momentum imbalance in inclusive and b -dijets as function of collision centrality in Pb+Pb collisions compared to pp . Figure is from Ref. [151]

The application of substructure techniques to heavy flavour jets in pp collisions has recently led to the first direct observation of the dead cone in QCD [152]. The exploration of such techniques in heavy ion collisions is yet to happen. Substructure of double HF-tagged jets (discussed in Ref. [153] in the context of disentangling heavy flavour processes in pp collisions) might allow to identify the $c\bar{c}$ or $b\bar{b}$ antenna without the ambiguities of the inclusive SD analysis that are subject of strong contamination of combinatorial prongs.

Heavy quark measurements are expected to be substantially improved in the near future with higher luminosity and detector upgrades at the LHC Runs 3 and 4 [154] and the ability to tag b -jets at sPHENIX at RHIC [155].

Does jet quenching depend on the hard substructure?

As described in Section 3.2, the grooming procedure stops when the SD condition is met. The corresponding z_{12} and angular separation ΔR_{12} are called groomed momentum balance and groomed jet radius and are denoted by z_g and R_g respectively.

In vacuum, z_g is connected to the Altarelli-Parisi splitting function and displays a universal behavior in $1/z$ [156]. In Pb-Pb collisions, the interpretation of the observable is more difficult because medium-induced radiation is expected to violate angular ordering [31] while the CA reclustering forces angular ordering on the jet constituents, among other reasons.

Several different mechanisms can contribute to the modification of z_g and R_g in heavy ion collisions. If medium-induced radiation is hard enough, it can increase the number of prongs that pass the SD cut. On the other hand, jet prongs and constituents lose energy in the medium, which can reduce the number of subjet prongs passing the SD cut, n_{SD} . In addition, the amount of jet energy loss is dictated by color coherence: jets with a resolved substructure will lose more energy because they contain more prongs that interact with the medium incoherently.

The z_g distribution in heavy-ion collisions was first measured by CMS [157], then by STAR [81] and ALICE [158]. The CMS and ALICE measurements are shown in Figure 11. The main feature of the ALICE track-based measurement was a suppression of the z_g distribution with increasing R_g and a hint of an enhancement at small angles. CMS did not perform a scan on the splitting opening angle (the default value is $R_g > 0.1$) but did examine the jet p_T dependence of the modification. Both of these measurements were not fully corrected to particle-level. Rather, the pp reference was modified to consider the impact of strong combinatorial background at the level of subjet prongs that dominates the low- z_g region. ALICE also reported the measurement of the Les Houches multiplicity n_{SD} which gives the number of prongs within the jet that pass the SD cut. The n_{SD} distribution is shifted to lower values in PbPb relative to the vacuum calculation as expected if energy loss of the prongs reduces the number of subleading prongs passing the SD cut.

The next generation of groomed observables by ALICE were fully corrected and, for the sake of the unfolding stability, performed with a different selection of smaller jet R and tighter SD grooming cuts ($z_{cut} = 0.2, z_{cut} = 0.4$) [159]. The results are shown in Figure 12. A similar message is distilled: small-angle splittings are enhanced while large-angle splittings are suppressed. And the z_g , when integrating over all angles, shows no modifications.

The data were compared to a set of models, including JetMed (denoted as Caucal et al), the Hybrid model (denoted as Pablos et al) and JETSCAPE [160]. The narrowing of θ_g is observed in these three different models, and this might seem surprising given the different nature of the implemented medium effects. So it is worth asking what is the most relevant common feature in these models, and one answer is the dominance of vacuum physics at early, high-energy stages of the shower [161, 162]. This brings in a key element for the interpretation: large θ_g biases to more activity

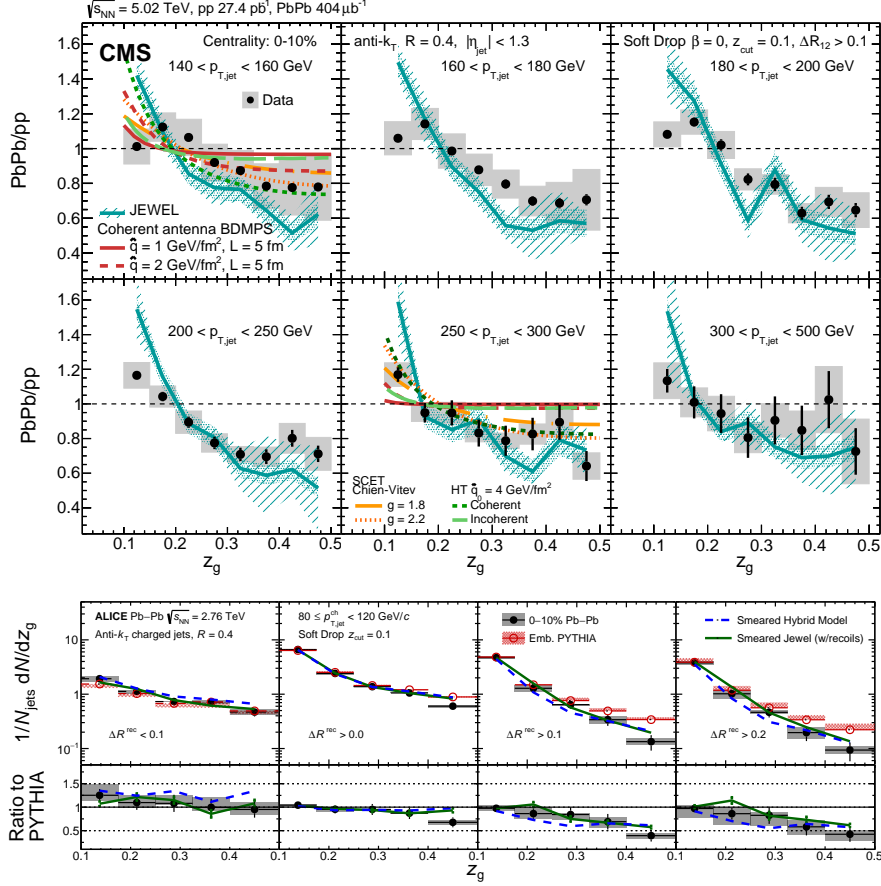


Figure 11: Upper plot: CMS self-normalized results for the momentum balance z_g in different jet momentum bins. Figure is from Ref. [157]. Lower plot: ALICE z_g results for jets in a fixed momentum interval of $80 < p_{T,jet}^{ch} < 120$ GeV and as function of the groomed splitting angle R_g (ΔR^{rec}). Figure is from Ref. [158].

in the early vacuum shower. Since vacuum structures with more prongs lead to more quenched jets, the shape of θ_g is the consequence of a selection bias; high θ_g jets are more quenched and migrate to lower jet p_T bins. Other models in the plot like the one denoted by Yuan et al indicate that flavour-dependent energy loss can also play a role.

Another substructure observable of interest is the N -subjettiness, denoted by τ_N , which quantifies the degree to which a jet has a N (or fewer)-pronged substructure [163]. The ratio of τ_2/τ_1 is used to tag boosted hadronically-decaying objects such as the W and top quarks, which are typically 2-prong objects as compared to

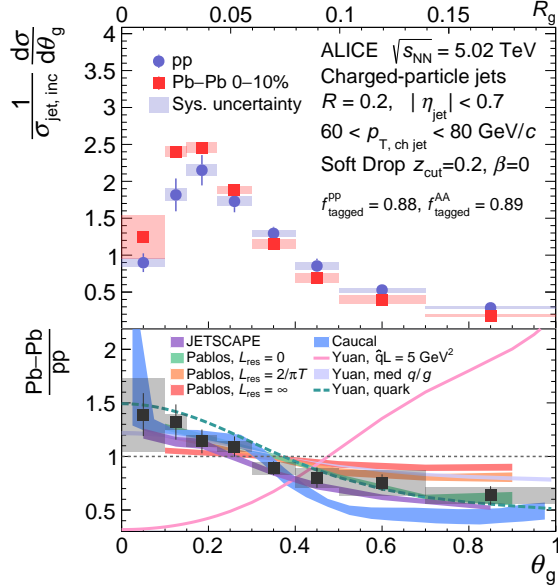


Figure 12: Normalized groomed jet radius θ_g in central collisions and small- R jets measured by ALICE [159], compared to the same observable measured in pp collisions and state of the art model and theory calculations.

QCD jets, which are mostly 1-pronged. ALICE measured τ_2/τ_1 [164] using several declustering metrics, including exclusive k_T and CA+SD. The results do not reveal a significant change in the prong-structure of the jet relative to PYTHIA, which describes the observable well in pp collisions.

ATLAS performed the first fully corrected measurement of the k_T distance of large- R jets in heavy ion collisions [165]. First, $R = 0.2$ calorimeter jets were reconstructed via the usual procedure. Then jets with $p_T^{\text{jet}} > 35$ GeV jets were taken as constituents for anti- k_T jets clustered with $R = 1$. Their constituents were reclustered with the k_T algorithm [91, 92] and then the last clustering step was unwound to register the k_T scale or distance, defined as

$$\sqrt{d_{12}} = \min(p_{T,1}^2, p_{T,2}^2) \Delta R_{12}^2 \quad (9)$$

where indexes 1 and 2 refer to the two prongs that were clustered last. Large $\sqrt{d_{12}}$ selects jets with distinct hard prongs separated at large angles. If an $R = 1$ jet consists of only a single sub-jet (SSJ), $\sqrt{d_{12}}$ is not defined. Figure 13 shows the k_T distance distribution for different centralities and indicates that the majority of the jets consist of a single sub-jet. Two-prong configurations are suppressed by more

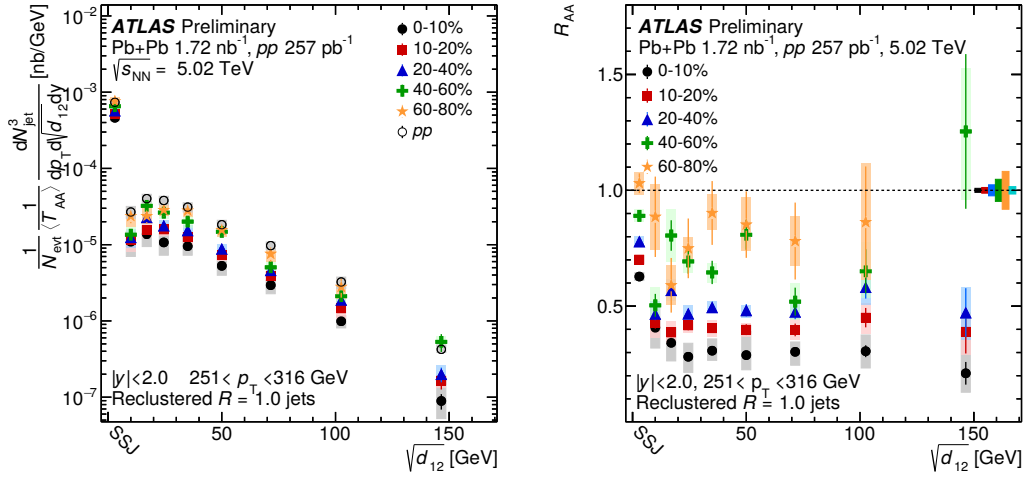


Figure 13: Left: Fully corrected k_T distance measured for $R = 1$ trimmed jets in the range $251 < p_{T,jet} < 316$ GeV for different centrality classes. Right: Nuclear modification factor as function of the k_T distance. Figures are from Ref. [165].

than 2 orders of magnitude.

The plot on the right shows the nuclear modification factor is qualitatively different between those jets which have a single sub-jet and those which have more than one. Those jets with a single sub-jet are suppressed approximately 50% less in central collisions than those jets which have multiple sub-jets.

In parallel to the writing of this review, other observables are being explored. An example is the subjet energy fraction, which considers the fraction of energy carried by the leading subjet within the signal jet. Another example is the transverse momentum k_T of the splitting found with dynamical grooming [95], $k_{T,\text{dyn}}$, which selects the hardest splitting within the CA-ordered jet tree.

All the discussed jet shape and jet substructure observables must be correlated to some degree, by construction. For illustration, in Fig. 14 we show the linear correlation coefficients for PYTHIA8 [166] jets reconstructed with $R = 0.4$ with $p_T^{\text{jet}} > 100$ GeV. We observe that the k_T distance is strongly correlated to the girth and to $k_{T,\text{dyn}}$ and strongly anti-correlated to the leading subjet fraction. The n_{SD} , which is a measure of the intrajet multiplicity is naturally anti-correlated to the p_{TD} which is related to the dispersion in momentum of the jet constituents. The z_g measures a momentum balance while R_g is an angle and they are not correlated. We also note the strong correlation between the girth and R_g , $k_{T,\text{dyn}}$, and the k_T distance. Finding a set of minimally correlated observables can be useful to perform

systematic comparisons to models and calculations. An example of such procedure in pp collisions is the recent extraction of α_S using jet substructure in $t\bar{t}$ events by CMS, where R_g, z_g, ϵ and jet multiplicity were identified as a set of minimally correlated variables among more than 30 substructure observables [167].

The selection bias was discussed in the context of the R_g but applies to most of the discussed observables. In order to mitigate this selection bias, and to increase the weight of quenched jets in the measured samples, different strategies are envisaged. An obvious one considers the substructure of jets recoiling from Z or γ bosons. Other interesting approaches based on ML have been proposed [161].

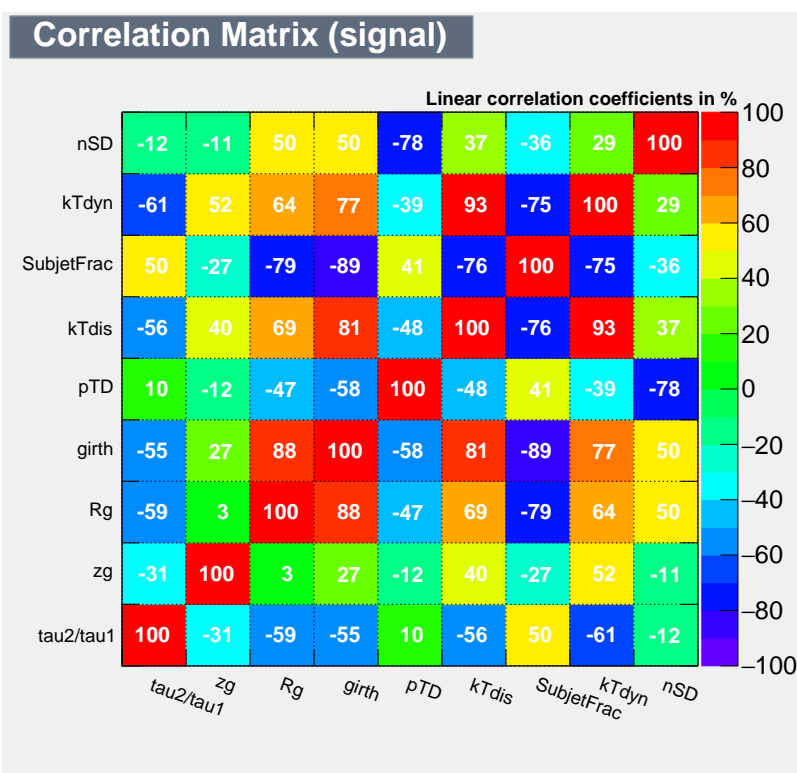


Figure 14: Linear Correlation matrix of the different jet shapes and substructure observables discussed in this chapter.

4.1.4 What happens to the energy lost from jets in the QGP?

The main physics aim here is to understand the process by which energy lost by the jet is incorporated into the QGP. There are two reasons why this is important:

- this provides access to the hydrodynamization process
- the energy from the medium response is correlated with the jet and affects other observables which are used to quantify the strength of energy loss [60, 168].

Three kinds of observables have been used to search for this effect:

- cone size dependence of jet R_{AA}
- correlations between jets and tracks
- fragmentation functions and jet shapes

In order to capture the full dynamics of jet quenching, large- R jets and access to their internal structure is desired. Cross sections and the ratios of cross sections for different R are IRC-safe observables that can be analytically calculated and pose strong constraints to the theory. The heavy-ion underlying event creates combinatorial or fake jets that prevent unfolding and only at very high jet p_T the measurement of the inclusive large- R jet is feasible. Below 100 GeV, the different collaborations have measured jet cross sections and their ratios for different R up to $R = 0.5$ [82, 169].

In the energy range of a few hundred GeV up to the 1 TeV, CMS has reported the first measurement of jet nuclear modification factors for jets with radii from $R = 0.2$ up to $R = 1$, for different centrality classes. In central collisions, and up to $R = 0.4$ (where there are still sufficient data points to observe a trend), the nuclear modification factor increases with jet p_T , in agreement with the ATLAS result for $R = 0.4$ jets [170]. Above 500 GeV, where a full scan of the R dependence is possible, the data is consistent with no dependence of the R_{AA} with jet R . The comparison of the data to models and calculations reveals significant tensions in the simultaneous description of the nuclear modification factor and its R dependence. In Fig. 15 an example of comparisons to analytical calculations is shown.

What is common to many of the models compared to the CMS data, is the strong role of the medium response which gives a larger contribution at large R . In models like the Hybrid model, the R dependence of R_{AA} can be explained as the result of the balance of a stronger suppression for broader jets, and the ability to include more medium response inside the cone. The high transverse momentum of the $R = 1.0$ jets in the CMS measurement could limit the effect of medium response. Measurements with a larger kinematic range will allow for better discrimination between models.

Other measurement that emphasizes the role of the medium response at large R is for instance the jet mass [171] for $R = 0.4$ jets. No modifications in Pb+Pb collisions

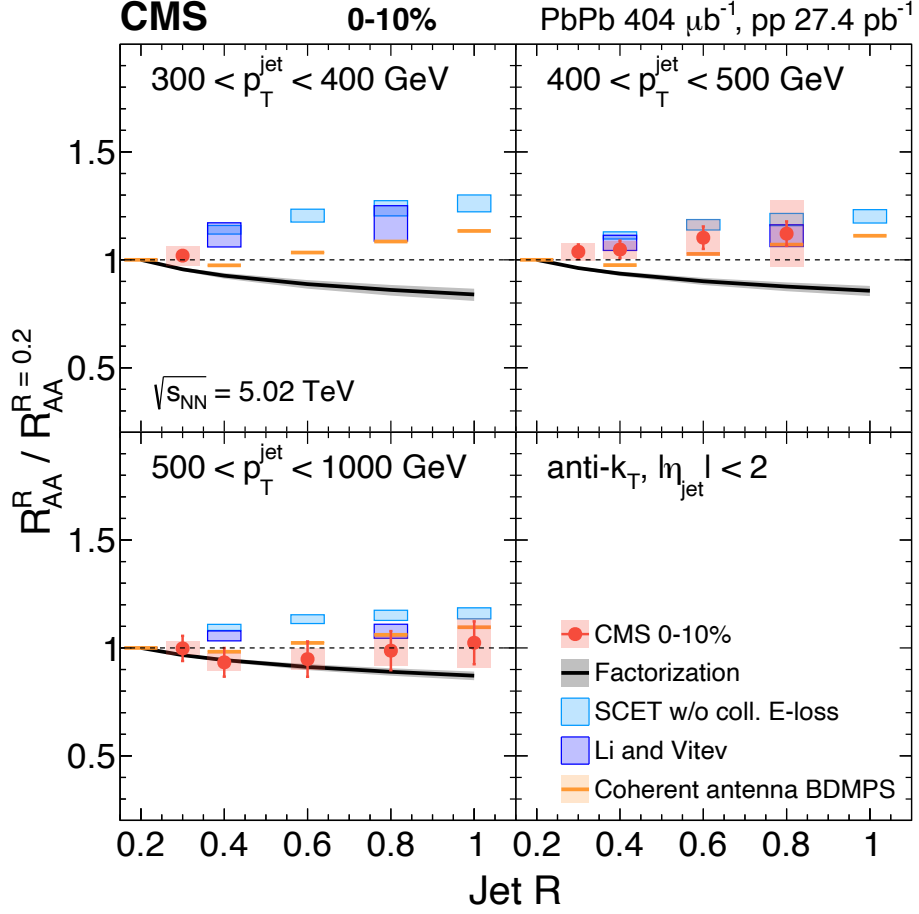


Figure 15: Ratio of the R_{AA} for different jet R and R_{AA} for $R = 0.2$, in different jet p_T intervals and compared to several calculations. Fig. from Ref. [173].

relative to p +Pb collisions were observed, possibly due to a balance of energy loss and medium response effects [172].

In order to look for medium response, measurements of low momentum tracks around jets in heavy-ion collisions have been performed. There has been interest in measuring fragmentation functions as a function of p_T^{part} , the transverse momentum of the particle in the jet. This is motivated to search for an absolute scale in the modification of the fragmentation. When looking at the jets fragmentation functions plotted as a function of p_T^{part} , the low- p_T^{part} , $p_T^{\text{part}} < 4$ GeV, part of these ratios are approximately equal for the three jet p_T selections. The low- p_T^{part} excess is thought

to be due to the response of the medium to the passage of the jet. The approximate scaling and extent in p_T^{part} of the excess would be then sensitive to some scale in the QGP associated with the response.

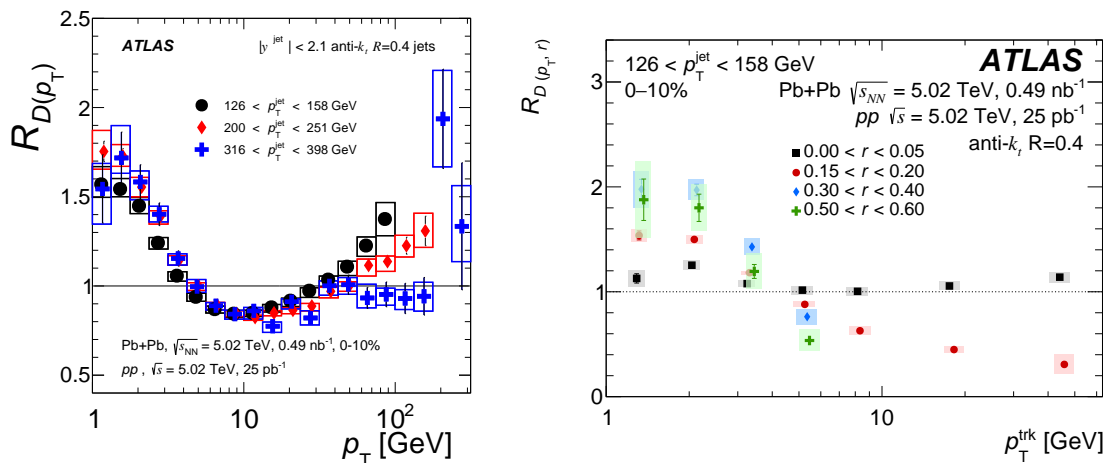


Figure 16: Left: Ratios of the fragmentation functions in central Pb+Pb collisions to those in pp collisions for three different p_T^{jet} selections as a function of charged-particle p_T . Right: The same quantity as in the left plot only differential in the distance, r , from the jet axis as well (different sets of points). Figures are from Ref. [129] (left) and [174] (right).

In order to study both the angular and longitudinal directions at once, both CMS and ATLAS have measured two-dimensional fragmentation functions [175, 176, 177, 174, 178]. In the longitudinal fragmentation functions we noted that the low- p_T^{part} excess was for particles below approximately 4 GeV. The two-dimensional fragmentation functions in Refs. [175, 177, 174] provide support for that approximate scale both in 2.76 and 5.02 TeV Pb+Pb collisions at the LHC. Figure 16 shows the ratio of the two-dimensional fragmentation function in central Pb+Pb collisions to that in pp collisions as a function of p_T^{part} for different values of distance r to the jet axis. The magnitude of the modifications changes as a function of r , but the location in p_T^{part} of the transition from suppression to enhancement is at approximately 4 GeV for all r values. This same 4 GeV scale is also seen in measurements of Z -hadron correlations at ATLAS [179].

4.2 Effective Degrees of Freedom of the QGP

The QGP behaves macroscopically as an almost perfect liquid. However, since the underlying theory is Quantum Chromodynamics, it is expected that if the QGP is probed at sufficiently short distances, the quasi-particle degrees of freedom will emerge [180]. If the QGP were strongly coupled at all scales, the distribution of transverse momentum k_T transferred from the medium to an energetic quark or gluon projectile is expected to be Gaussian. In the limit where the parton projectile resolves the free quarks and gluons within the QGP, the distribution of transferred transverse momentum is expected to follow a power-law tail $1/k_{T,4}$, typical of point-like scatterers. This is often referred to as the Molière regime.

The searches for point-like scatterers in the QGP can be done both at inter-jet and intra-jet level. In the inter-jet case, the azimuthal correlation between a high-pt hadron, or ideally a photon or a boson and the recoiling jet is measured and compared the yield of large-angle deflections in Pb+Pb and pp collisions in the search for an excess. The intra-jet case utilizes new substructure techniques in order to identify high- k_T prongs or splittings within the jet. An example of such techniques is the dynamical grooming [181], which allows to select the hardest prong in the jet tree. New NLO calculations of the medium-induced radiative spectrum within the Improved Opacity Expansion [44] and their ongoing extension to substructure will provide analytical reference to the expected impact of the power-law tail.

Inter-jet azimuthal correlations have been studied by ATLAS [182], CMS [183], ALICE [169] and STAR [83] collaborations in different kinematic regimes. As an example, the ALICE semi-inclusive azimuthal correlation between high-momentum hadrons and jets is shown in Figure 17, together with the accumulated integrated yield on the right plot. The statistical precision of the data doesn't allow conclusions to be drawn on a possible modification of the yield at very large angles. However the ALICE measurements sketches what can be done in the near future with higher statistics, with a pp reference instead of a MC calculation and with a full and simultaneous correction of the recoil jet momentum and the azimuthal angle and a full kinematic scan of the trigger object (ideally a photon) and the recoil jet p_T . The CMS measurement of the azimuthal correlation between isolated photons and jets is shown in Figure 18. The sensitivity to large-angle modifications is limited by statistics and by the systematics of the uncorrelated background subtraction.

This section focuses on the tails of the azimuthal correlation, but the bulk of the correlation is also of interest to probe broadening due to multiple soft scatterings with the medium. Calculations have shown that the sensitivity to medium effects is enhanced at low photon and recoil jet energies, since at high energies the distribution is dominated by vacuum radiation [184] and medium effects are indistinguishable.

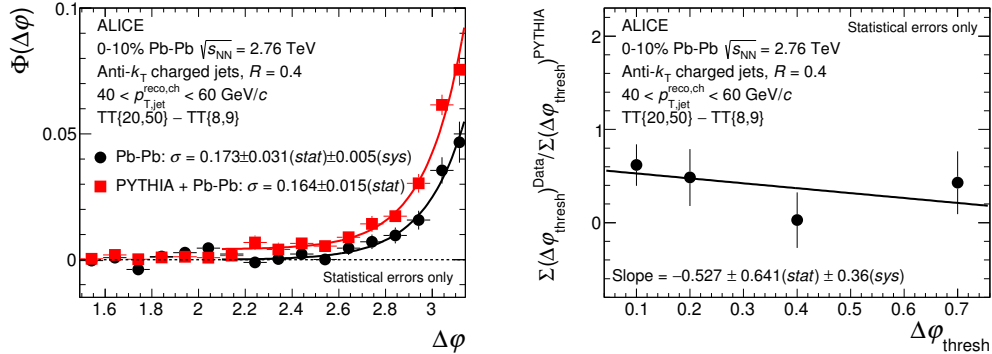


Figure 17: From Ref. [169] Left: Azimuthal correlation between a high- p_T hadron and the recoiling jets in Pb-Pb collisions and in the vacuum PYTHIA calculation. Right: Large-angle deflections are examined by integrating the yield of the azimuthal correlation from $\pi/2$ to $\pi - \varphi_{\text{thresh}}$

4.3 Critical Size for QGP Formation

4.3.1 Searches for Jet Quenching in pA collisions

Given the recent wealth of data showing evidence for collective behavior in $p+\text{Pb}$, pp collisions (for a recent review see Ref. [185]), it is natural to search for jet quenching effects in these systems. As of this writing no effects of jet quenching have been observed in $p+\text{Pb}$ or pp collisions. Here we discuss several searches for jet quenching in pA collisions.

The nuclear modification factor R_{pA} has been measured both in $d+\text{Au}$ collisions at RHIC and $p+\text{Pb}$ collisions at the LHC for both jets [186, 124, 187] and charged particles [188, 189, 125]. No evidence for jet quenching was found in these measurements. However, the precision of these measurements is limited by the normalization uncertainties associated with the nuclear modification factor coming from the luminosity and $\langle T_{AA} \rangle$ determination (along with other sources).

In order to be sensitive to potentially smaller jet quenching effects, measurements of self-normalized observables (e.g. normalized per-jet, or per-trigger particle) have been done. ALICE measured the charged-particle jets opposite to a high-transverse momentum trigger hadron [190] and reported their per-trigger normalized yield over a broad kinematic range. The advantage of the per trigger particle normalisation is that no $\langle T_{AA} \rangle$ scaling of the reference is needed and thus no Glauber modelling and interpretation of the event activity (EA) in terms of geometry is required. Events are classified according to how hits in a forward scintillator in the Pb-going direction

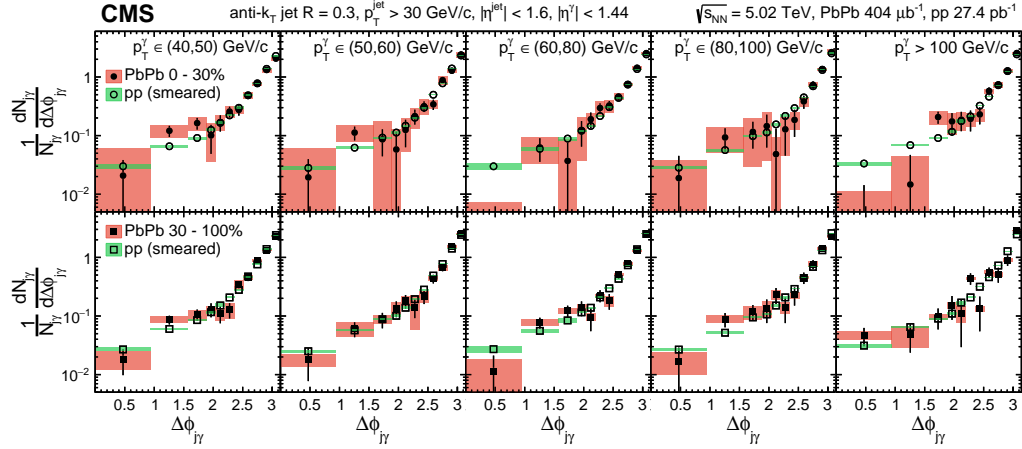


Figure 18: CMS gamma-jet azimuthal correlation in PbPb compared to pp collisions from Ref. [183]

or hits in a zero-degree neutron detector also in the Pb-going direction. Figure 19, shows the ratio of the observable in the two EA classes. The ratio is consistent with no energy loss. The red line indicates a limit, at 90% confidence level, on the average p_T shift of 0.4 GeV/ c , which is an estimate of the maximum energy that is transported outside the jet cone.

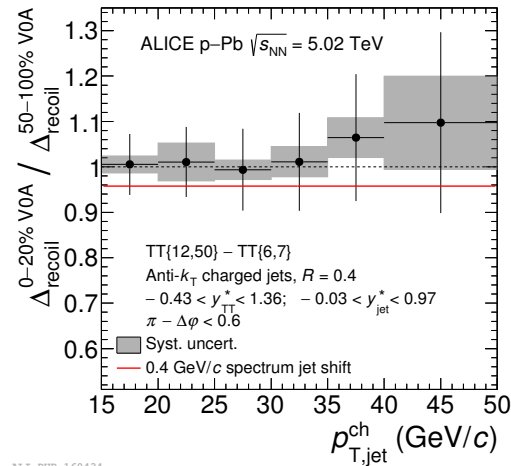


Figure 19: Ratio of recoil jet p_T distribution in $p+Pb$ events with high and low event activity measured in the forward detectors. From Ref. [191]

ATLAS measured fragmentation functions in p +Pb collisions [191]. As shown in Figure 20 in contrast to Pb+Pb collisions, no significant deviation was found between the p +Pb fragmentation functions and the pp ones for the soft particles in the jet. There is some excess of less than 10% in the central values for charged-particles between approximately 1–5 GeV between the fragmentation functions in p +Pb and pp collisions but it is within the size of the systematic uncertainties. Also shown in Figure 20 is the measurement from CMS of the dijet asymmetry in p +Pb collisions selected on the forward energy in the Pb-going direction [192]. They evaluated the mean of this distribution and found that quantity to be independent of the forward energy to within their uncertainties.

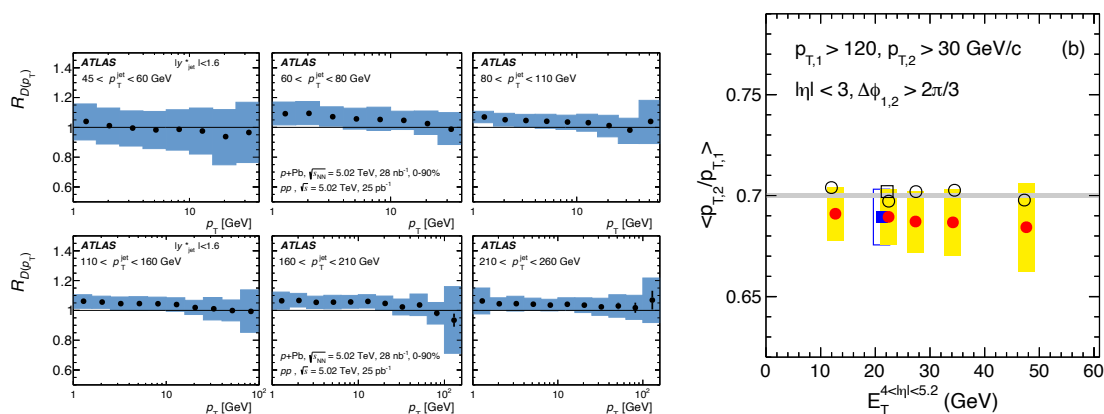


Figure 20: (left) Ratios of the fragmentation functions in p +Pb collisions to those in pp collisions for various p_T^{jet} selections as a function of charged particle p_T . (right) Mean value of the ratio of the subleading to leading $p_T^{\text{jet}}(x_J)$ as a function of the transverse energy in the Pb-going direction. Figures are from Ref. [191] (left) and Ref. [192] (right).

There is ongoing interest in more sensitive measurements which might be more sensitive to any jet quenching signal but the existing measurements clearly show that any jet quenching which might exist in p +Pb collisions is much smaller than that in heavy ion collisions.

4.3.2 Light ion collisions

In order to map the transition between large systems (e.g. central heavy ion collisions) with large energy loss and small pA systems without observed energy loss,

there is a lot of interest in having small, symmetric collision systems with which to potentially observe the turn-off of jet quenching.

Some data from collision systems smaller than Pb+Pb or Au+Au does exist. Most recently, the LHC delivered Xe+Xe collisions in 2017. Those results showed that the value of R_{AA} for charged particles depends primarily on the size of the collision system (as measured by the charged particle multiplicity) [193]. However, the utility of the Xe+Xe measurements to answer this question is limited by the fact that Xe+Xe collisions are much closer in charged-particle multiplicity and N_{part} to Pb+Pb collisions than they are to p +Pb collisions.

In light of this there remains a great interest in colliding a much smaller collision system, with an N_{part} close to that of p +Pb collisions but with a larger geometrical transverse overlap that increases the in-medium path length and thus potentially, quenching. The preferred collision system is O+O [194, 195]. The experimental projections for the nuclear modification factor of charged hadrons measured in a short O+O run of 0.5 nb^{-1} [196] were compared to theoretical expectations for jet quenching [194, 197]. The comparison indicates that partonic energy loss signal might be observed at transverse momentum of approximately 20 GeV.

In the spring of 2021 RHIC ran O+O collisions for the STAR experiment. The data from that run has not yet been analyzed but will be the first look at this important question.

5 Conclusions and Outlook

This review covers the current status of measurements which use jets to study the properties of the quark-gluon plasma. The initial observations of jet quenching at RHIC and later at the LHC were only the beginning of this rich program.

Measurements covered here clearly show that the amount of energy loss a jet undergoes depends on the structure of the jet. Broader jets and jets with a distinct two-prong substructure with a large opening angle appear to be more suppressed than inclusive jets. This observation clearly motivates further measurements sensitive to the jet flavor and substructure as essential to understanding the interactions between jets and the QGP. Among those measurements, the substructure of jets recoiling from a photon or Z-boson are of particular interest to mitigate the selection bias present in inclusive measurements.

Measurements have also shown that there is a wide distribution of soft particles around jets. This is thought to be from the response of the QGP to the jet passing through it. This can provide further information about the transport of energy in the QGP. Several of the measurements discussed in this review can be described as

a balance between energy loss, and the recovery of the medium response to the jet at large angles.

Finally, we have discussed measurements which show how jet quenching depends on geometry. More measurements sensitive to this, including the effects of fluctuations in the initial geometry of the collision are essential to understand the path length dependence of energy loss.

The limit of jet quenching in very small QGP systems is an area of great interest. Evidence for collectivity is well established in p +Pb collisions, however jet quenching has not been observed. Reconciling these measurements into a common interpretation is a key physics aim of the light-ion program underway at RHIC and expected in Run 3 (2024) at the LHC.

Looking forward we anticipate a few exciting opportunities in this field in the next few years. First, there are exciting experimental and theoretical investigations into jet substructure ongoing. These will be key in understanding how energy loss happens. Second there will be a wealth of new data, including Run 3 at the LHC with increased luminosity and the first data taken with the ALICE upgrades and the turn on of sPHENIX at RHIC. sPHENIX will provide fully calorimetric jets at RHIC for the first time and will have a data recording rate which will allow for a greatly expanded kinematic range of jets at RHIC. This will allow for new constraints on the dependence of jet quenching on the QGP temperature.

6 Acknowledgements

The authors thank Matthew Nguyen, Martin Rybar, Carlos Salgado, and Marco van Leeuwen for comments and suggestions to the draft. The authors also thank the ALICE, ATLAS, CMS, PHENIX and STAR Collaborations for the great experimental results. LCM is supported by the European Research Council project ERC-2020-COG-101002207 QCDHighDensityCMS. AMS acknowledges support from National Science Foundation Award Number 2111046.

7 References

References

- [1] Wit Busza, Krishna Rajagopal, and Wilke van der Schee. Heavy Ion Collisions: The Big Picture, and the Big Questions. *Ann. Rev. Nucl. Part. Sci.*, 68:339–376, 2018. [arXiv:1802.04801](https://arxiv.org/abs/1802.04801), [doi:10.1146/annurev-nucl-101917-020852](https://doi.org/10.1146/annurev-nucl-101917-020852).

- [2] I. Arsene et al. Quark gluon plasma and color glass condensate at RHIC? The Perspective from the BRAHMS experiment. *Nucl. Phys. A*, 757:1–27, 2005. [arXiv:nucl-ex/0410020](#), [doi:10.1016/j.nuclphysa.2005.02.130](#).
- [3] K. Adcox et al. Formation of dense partonic matter in relativistic nucleus-nucleus collisions at RHIC: Experimental evaluation by the PHENIX collaboration. *Nucl. Phys. A*, 757:184–283, 2005. [arXiv:nucl-ex/0410003](#), [doi:10.1016/j.nuclphysa.2005.03.086](#).
- [4] B. B. Back et al. The PHOBOS perspective on discoveries at RHIC. *Nucl. Phys. A*, 757:28–101, 2005. [arXiv:nucl-ex/0410022](#), [doi:10.1016/j.nuclphysa.2005.03.084](#).
- [5] John Adams et al. Experimental and theoretical challenges in the search for the quark gluon plasma: The STAR Collaboration’s critical assessment of the evidence from RHIC collisions. *Nucl. Phys. A*, 757:102–183, 2005. [arXiv:nucl-ex/0501009](#), [doi:10.1016/j.nuclphysa.2005.03.085](#).
- [6] G. Roland, K. Safarik, and P. Steinberg. Heavy-ion collisions at the LHC. *Prog. Part. Nucl. Phys.*, 77:70–127, 2014. [doi:10.1016/j.ppnp.2014.05.001](#).
- [7] Ulrich Heinz and Raimond Snellings. Collective flow and viscosity in relativistic heavy-ion collisions. *Ann. Rev. Nucl. Part. Sci.*, 63:123–151, 2013. [arXiv:1301.2826](#), [doi:10.1146/annurev-nucl-102212-170540](#).
- [8] Jaroslav Adam et al. Direct photon production in Pb-Pb collisions at $\sqrt{s_{\text{NN}}} = 2.76$ TeV. *Phys. Lett. B*, 754:235–248, 2016. [arXiv:1509.07324](#), [doi:10.1016/j.physletb.2016.01.020](#).
- [9] P. Kovtun, Dan T. Son, and Andrei O. Starinets. Viscosity in strongly interacting quantum field theories from black hole physics. *Phys. Rev. Lett.*, 94:111601, 2005. [arXiv:hep-th/0405231](#), [doi:10.1103/PhysRevLett.94.111601](#).
- [10] Allan Adams, Lincoln D. Carr, Thomas Schäfer, Peter Steinberg, and John E. Thomas. Strongly Correlated Quantum Fluids: Ultracold Quantum Gases, Quantum Chromodynamic Plasmas, and Holographic Duality. *New J. Phys.*, 14:115009, 2012. [arXiv:1205.5180](#), [doi:10.1088/1367-2630/14/11/115009](#).
- [11] Juan Martin Maldacena. The Large N limit of superconformal field theories and supergravity. *Adv. Theor. Math. Phys.*, 2:231–252, 1998. [arXiv:hep-th/9711200](#), [doi:10.1023/A:1026654312961](#).

- [12] Ani Aprahamian et al. Reaching for the horizon: The 2015 long range plan for nuclear science. 10 2015.
- [13] Richard Keith Ellis et al. Physics Briefing Book: Input for the European Strategy for Particle Physics Update 2020. 10 2019. [arXiv:1910.11775](#).
- [14] M. Aaboud et al. Measurement of inclusive jet and dijet cross-sections in proton-proton collisions at $\sqrt{s} = 13$ TeV with the ATLAS detector. *JHEP*, 05:195, 2018. [arXiv:1711.02692](#), [doi:10.1007/JHEP05\(2018\)195](#).
- [15] Vardan Khachatryan et al. Measurement of the double-differential inclusive jet cross section in proton-proton collisions at $\sqrt{s} = 13$ TeV. *Eur. Phys. J. C*, 76(8):451, 2016. [arXiv:1605.04436](#), [doi:10.1140/epjc/s10052-016-4286-3](#).
- [16] Simone Marzani, Gregory Soyez, and Michael Spannowsky. *Looking inside jets: an introduction to jet substructure and boosted-object phenomenology*, volume 958. Springer, 2019. [arXiv:1901.10342](#), [doi:10.1007/978-3-030-15709-8](#).
- [17] J. D. Bjorken. Energy Loss of Energetic Partons in Quark - Gluon Plasma: Possible Extinction of High p(t) Jets in Hadron - Hadron Collisions. 8 1982.
- [18] Miklos Gyulassy and Michael Plumer. Jet Quenching in Dense Matter. *Phys. Lett. B*, 243:432–438, 1990. [doi:10.1016/0370-2693\(90\)91409-5](#).
- [19] R. Baier, Yuri L. Dokshitzer, Alfred H. Mueller, S. Peigne, and D. Schiff. Radiative energy loss of high-energy quarks and gluons in a finite volume quark - gluon plasma. *Nucl. Phys. B*, 483:291–320, 1997. [arXiv:hep-ph/9607355](#), [doi:10.1016/S0550-3213\(96\)00553-6](#).
- [20] R. Baier, Yuri L. Dokshitzer, Alfred H. Mueller, S. Peigne, and D. Schiff. Radiative energy loss and p(T) broadening of high-energy partons in nuclei. *Nucl. Phys. B*, 484:265–282, 1997. [arXiv:hep-ph/9608322](#), [doi:10.1016/S0550-3213\(96\)00581-0](#).
- [21] B. G. Zakharov. Radiative energy loss of high-energy quarks in finite size nuclear matter and quark - gluon plasma. *JETP Lett.*, 65:615–620, 1997. [arXiv:hep-ph/9704255](#), [doi:10.1134/1.567389](#).
- [22] Miklos Gyulassy, Peter Levai, and Ivan Vitev. Jet quenching in thin quark gluon plasmas. 1. Formalism. *Nucl. Phys. B*, 571:197–233, 2000. [arXiv:hep-ph/9907461](#), [doi:10.1016/S0550-3213\(99\)00713-0](#).

- [23] Carlos A. Salgado and Urs Achim Wiedemann. Calculating quenching weights. *Phys. Rev. D*, 68:014008, 2003. [arXiv:hep-ph/0302184](#), doi:10.1103/PhysRevD.68.014008.
- [24] Peter Brockway Arnold, Guy D. Moore, and Laurence G. Yaffe. Photon emission from ultrarelativistic plasmas. *JHEP*, 11:057, 2001. [arXiv:hep-ph/0109064](#), doi:10.1088/1126-6708/2001/11/057.
- [25] Peter Brockway Arnold, Guy D. Moore, and Laurence G. Yaffe. Photon emission from quark gluon plasma: Complete leading order results. *JHEP*, 12:009, 2001. [arXiv:hep-ph/0111107](#), doi:10.1088/1126-6708/2001/12/009.
- [26] Peter Brockway Arnold, Guy D. Moore, and Laurence G. Yaffe. Photon and gluon emission in relativistic plasmas. *JHEP*, 06:030, 2002. [arXiv:hep-ph/0204343](#), doi:10.1088/1126-6708/2002/06/030.
- [27] Simon Caron-Huot and Charles Gale. Finite-size effects on the radiative energy loss of a fast parton in hot and dense strongly interacting matter. *Phys. Rev. C*, 82:064902, 2010. [arXiv:1006.2379](#), doi:10.1103/PhysRevC.82.064902.
- [28] Xin-Nian Wang and Xiao-feng Guo. Multiple parton scattering in nuclei: Parton energy loss. *Nucl. Phys. A*, 696:788–832, 2001. [arXiv:hep-ph/0102230](#), doi:10.1016/S0375-9474(01)01130-7.
- [29] A. Majumder and Berndt Muller. Higher twist jet broadening and classical propagation. *Phys. Rev. C*, 77:054903, 2008. [arXiv:0705.1147](#), doi:10.1103/PhysRevC.77.054903.
- [30] Yacine Mehtar-Tani, Carlos A. Salgado, and Konrad Tywoniuk. Anti-angular ordering of gluon radiation in QCD media. *Phys. Rev. Lett.*, 106:122002, 2011. [arXiv:1009.2965](#), doi:10.1103/PhysRevLett.106.122002.
- [31] Y. Mehtar-Tani, C. A. Salgado, and K. Tywoniuk. Jets in QCD Media: From Color Coherence to Decoherence. *Phys. Lett. B*, 707:156–159, 2012. [arXiv:1102.4317](#), doi:10.1016/j.physletb.2011.12.042.
- [32] Yacine Mehtar-Tani and Konrad Tywoniuk. Jet coherence in QCD media: the antenna radiation spectrum. *JHEP*, 01:031, 2013. [arXiv:1105.1346](#), doi:10.1007/JHEP01(2013)031.

- [33] J. Casalderrey-Solana and E. Iancu. Interference effects in medium-induced gluon radiation. *JHEP*, 08:015, 2011. arXiv:1105.1760, doi:10.1007/JHEP08(2011)015.
- [34] Nestor Armesto, Hao Ma, Yacine Mehtar-Tani, Carlos A. Salgado, and Konrad Tywoniuk. Mass effect and coherence in medium-induced QCD radiation off a $q\bar{q}$ antenna. *J. Phys. G*, 38:124140, 2011. arXiv:1107.0291, doi:10.1088/0954-3899/38/12/124140.
- [35] Nestor Armesto, Hao Ma, Yacine Mehtar-Tani, Carlos A. Salgado, and Konrad Tywoniuk. Coherence effects and broadening in medium-induced QCD radiation off a massive $q\bar{q}$ antenna. *JHEP*, 01:109, 2012. arXiv:1110.4343, doi:10.1007/JHEP01(2012)109.
- [36] Yacine Mehtar-Tani, Carlos A. Salgado, and Konrad Tywoniuk. The Radiation pattern of a QCD antenna in a dense medium. *JHEP*, 10:197, 2012. arXiv:1205.5739, doi:10.1007/JHEP10(2012)197.
- [37] Jorge Casalderrey-Solana, Yacine Mehtar-Tani, Carlos A. Salgado, and Konrad Tywoniuk. New picture of jet quenching dictated by color coherence. *Phys. Lett. B*, 725:357–360, 2013. arXiv:1210.7765, doi:10.1016/j.physletb.2013.07.046.
- [38] Peter Arnold and Shahin Iqbal. The LPM effect in sequential bremsstrahlung. *JHEP*, 04:070, 2015. [Erratum: *JHEP* 09, 072 (2016)]. arXiv:1501.04964, doi:10.1007/JHEP09(2016)072.
- [39] Peter Arnold, Han-Chih Chang, and Shahin Iqbal. The LPM effect in sequential bremsstrahlung 2: factorization. *JHEP*, 09:078, 2016. arXiv:1605.07624, doi:10.1007/JHEP09(2016)078.
- [40] Peter Arnold, Tyler Gorda, and Shahin Iqbal. The LPM effect in sequential bremsstrahlung: nearly complete results for QCD. *JHEP*, 11:053, 2020. arXiv:2007.15018, doi:10.1007/JHEP11(2020)053.
- [41] L.D. Landau and I.Ya. Pomeranchuk. Sudakov suppression of jets in QCD media. *Kokl.Akad.Nauk SSSR*, 92(535):735, 1953.
- [42] Carlota Andres, Liliana Apolinário, and Fabio Dominguez. Medium-induced gluon radiation with full resummation of multiple scatterings for realistic parton-medium interactions. *JHEP*, 07:114, 2020. arXiv:2002.01517, doi:10.1007/JHEP07(2020)114.

- [43] Xabier Feal and Ricardo Vazquez. Intensity of gluon bremsstrahlung in a finite plasma. *Phys. Rev. D*, 98(7):074029, 2018. arXiv:1811.01591, doi:10.1103/PhysRevD.98.074029.
- [44] João Barata, Yacine Mehtar-Tani, Alba Soto-Ontoso, and Konrad Tywoniuk. Medium-induced radiative kernel with the Improved Opacity Expansion. 6 2021. arXiv:2106.07402.
- [45] Yacine Mehtar-Tani and Konrad Tywoniuk. Improved opacity expansion for medium-induced parton splitting. *JHEP*, 06:187, 2020. arXiv:1910.02032, doi:10.1007/JHEP06(2020)187.
- [46] Yacine Mehtar-Tani, Daniel Pablos, and Konrad Tywoniuk. Cone size dependence of jet suppression in heavy-ion collisions. 1 2021. arXiv:2101.01742.
- [47] Christian W. Bauer, Sean Fleming, Dan Pirjol, and Iain W. Stewart. An Effective field theory for collinear and soft gluons: Heavy to light decays. *Phys. Rev. D*, 63:114020, 2001. arXiv:hep-ph/0011336, doi:10.1103/PhysRevD.63.114020.
- [48] Ahmad Idilbi and Abhijit Majumder. Extending Soft-Collinear-Effective-Theory to describe hard jets in dense QCD media. *Phys. Rev. D*, 80:054022, 2009. arXiv:0808.1087, doi:10.1103/PhysRevD.80.054022.
- [49] Grigory Ovanesyan and Ivan Vitev. An effective theory for jet propagation in dense QCD matter: jet broadening and medium-induced bremsstrahlung. *JHEP*, 06:080, 2011. arXiv:1103.1074, doi:10.1007/JHEP06(2011)080.
- [50] Yang-Ting Chien and Ivan Vitev. Probing the Hardest Branching within Jets in Heavy-Ion Collisions. *Phys. Rev. Lett.*, 119(11):112301, 2017. arXiv:1608.07283, doi:10.1103/PhysRevLett.119.112301.
- [51] Yang-Ting Chien and Ivan Vitev. Towards the understanding of jet shapes and cross sections in heavy ion collisions using soft-collinear effective theory. *JHEP*, 05:023, 2016. arXiv:1509.07257, doi:10.1007/JHEP05(2016)023.
- [52] Paul Caucal. Jet evolution in a dense QCD medium. Other thesis, 10 2020. arXiv:2010.02874.
- [53] Korinna C. Zapp. JEWEL 2.0.0: directions for use. *Eur. Phys. J. C*, 74(2):2762, 2014. arXiv:1311.0048, doi:10.1140/epjc/s10052-014-2762-1.

- [54] Bjoern Schenke, Charles Gale, and Sangyong Jeon. MARTINI: An Event generator for relativistic heavy-ion collisions. *Phys. Rev. C*, 80:054913, 2009. [arXiv:0909.2037](#), [doi:10.1103/PhysRevC.80.054913](#).
- [55] Amit Kumar et al. Jet quenching in a multi-stage Monte Carlo approach. *Nucl. Phys. A*, 1005:122009, 2021. [arXiv:2002.07124](#), [doi:10.1016/j.nuclphysa.2020.122009](#).
- [56] N. Armesto, L. Cunqueiro, and C. A. Salgado. Implementation of a medium-modified parton shower algorithm. *Eur. Phys. J. C*, 61:775–778, 2009. [arXiv:0809.4433](#), [doi:10.1140/epjc/s10052-008-0824-y](#).
- [57] Thorsten Renk. YaJEM: a Monte Carlo code for in-medium shower evolution. *Int. J. Mod. Phys. E*, 20:1594–1599, 2011. [arXiv:1009.3740](#), [doi:10.1142/S0218301311019933](#).
- [58] I. P. Lokhtin, A. V. Belyaev, and A. M. Snigirev. Jet quenching pattern at LHC in PYQUEN model. *Eur. Phys. J. C*, 71:1650, 2011. [arXiv:1103.1853](#), [doi:10.1140/epjc/s10052-011-1650-1](#).
- [59] Xin-Nian Wang and Yan Zhu. Medium Modification of γ -jets in High-energy Heavy-ion Collisions. *Phys. Rev. Lett.*, 111(6):062301, 2013. [arXiv:1302.5874](#), [doi:10.1103/PhysRevLett.111.062301](#).
- [60] Yayun He, Shanshan Cao, Wei Chen, Tan Luo, Long-Gang Pang, and Xin-Nian Wang. Interplaying mechanisms behind single inclusive jet suppression in heavy-ion collisions. *Phys. Rev. C*, 99(5):054911, 2019. [arXiv:1809.02525](#), [doi:10.1103/PhysRevC.99.054911](#).
- [61] Yayun He, Tan Luo, Xin-Nian Wang, and Yan Zhu. Linear Boltzmann Transport for Jet Propagation in the Quark-Gluon Plasma: Elastic Processes and Medium Recoil. *Phys. Rev. C*, 91:054908, 2015. [Erratum: *Phys.Rev.C* 97, 019902 (2018)]. [arXiv:1503.03313](#), [doi:10.1103/PhysRevC.91.054908](#).
- [62] Shanshan Cao and Xin-Nian Wang. Jet quenching and medium response in high-energy heavy-ion collisions: a review. *Rept. Prog. Phys.*, 84(2):024301, 2021. [arXiv:2002.04028](#), [doi:10.1088/1361-6633/abc22b](#).
- [63] Paul M. Chesler and Krishna Rajagopal. Jet quenching in strongly coupled plasma. *Phys. Rev. D*, 90(2):025033, 2014. [arXiv:1402.6756](#), [doi:10.1103/PhysRevD.90.025033](#).

- [64] Jorge Casalderrey-Solana, Doga Can Gulhan, José Guilherme Milhano, Daniel Pablos, and Krishna Rajagopal. A Hybrid Strong/Weak Coupling Approach to Jet Quenching. *JHEP*, 10:019, 2014. [Erratum: *JHEP* 09, 175 (2015)]. arXiv:1405.3864, doi:10.1007/JHEP09(2015)175.
- [65] Guang-You Qin and Xin-Nian Wang. Jet quenching in high-energy heavy-ion collisions. *Int. J. Mod. Phys. E*, 24(11):1530014, 2015. arXiv:1511.00790, doi:10.1142/S0218301315300143.
- [66] Jean-Paul Blaizot and Yacine Mehtar-Tani. Jet Structure in Heavy Ion Collisions. *Int. J. Mod. Phys. E*, 24(11):1530012, 2015. arXiv:1503.05958, doi:10.1142/S021830131530012X.
- [67] Jorge Casalderrey-Solana and Carlos A. Salgado. Introductory lectures on jet quenching in heavy ion collisions. *Acta Phys. Polon. B*, 38:3731–3794, 2007. arXiv:0712.3443.
- [68] Matteo Cacciari, Gavin P. Salam, and Gregory Soyez. The anti- k_t jet clustering algorithm. *JHEP*, 04:063, 2008. arXiv:0802.1189, doi:10.1088/1126-6708/2008/04/063.
- [69] Matteo Cacciari, Gavin P. Salam, and Gregory Soyez. FastJet User Manual. *Eur. Phys. J. C*, 72:1896, 2012. arXiv:1111.6097, doi:10.1140/epjc/s10052-012-1896-2.
- [70] Matteo Cacciari, Gavin P. Salam, and Gregory Soyez. The Catchment Area of Jets. *JHEP*, 04:005, 2008. arXiv:0802.1188, doi:10.1088/1126-6708/2008/04/005.
- [71] Georges Aad et al. Measurement of soft-drop jet observables in pp collisions with the ATLAS detector at $\sqrt{s} = 13$ TeV. *Phys. Rev. D*, 101(5):052007, 2020. arXiv:1912.09837, doi:10.1103/PhysRevD.101.052007.
- [72] Hsi-Ming Chang, Massimiliano Procura, Jesse Thaler, and Wouter J. Waalewijn. Calculating Track-Based Observables for the LHC. *Phys. Rev. Lett.*, 111:102002, 2013. arXiv:1303.6637, doi:10.1103/PhysRevLett.111.102002.
- [73] Georges Aad et al. Jet energy measurement and its systematic uncertainty in proton-proton collisions at $\sqrt{s} = 7$ TeV with the ATLAS detector. *Eur. Phys. J. C*, 75:17, 2015. arXiv:1406.0076, doi:10.1140/epjc/s10052-014-3190-y.

- [74] D. Buskulic et al. Performance of the ALEPH detector at LEP. *Nucl. Instrum. Meth. A*, 360:481–506, 1995. doi:10.1016/0168-9002(95)00138-7.
- [75] A. M. Sirunyan et al. Particle-flow reconstruction and global event description with the CMS detector. *JINST*, 12(10):P10003, 2017. arXiv:1706.04965, doi:10.1088/1748-0221/12/10/P10003.
- [76] Matteo Cacciari and Gavin P. Salam. Pileup subtraction using jet areas. *Phys. Lett. B*, 659:119–126, 2008. arXiv:0707.1378, doi:10.1016/j.physletb.2007.09.077.
- [77] Gregory Soyez, Gavin P. Salam, Jihun Kim, Souvik Dutta, and Matteo Cacciari. Pileup subtraction for jet shapes. *Phys. Rev. Lett.*, 110(16):162001, 2013. arXiv:1211.2811, doi:10.1103/PhysRevLett.110.162001.
- [78] Jet energy scale and its uncertainty for jets reconstructed using the ATLAS heavy ion jet algorithm. 4 2015.
- [79] Peter Berta, Martin Spousta, David W. Miller, and Rupert Leitner. Particle-level pileup subtraction for jets and jet shapes. *JHEP*, 06:092, 2014. arXiv:1403.3108, doi:10.1007/JHEP06(2014)092.
- [80] P. Berta, L. Masetti, D. W. Miller, and M. Spousta. Pileup and Underlying Event Mitigation with Iterative Constituent Subtraction. *JHEP*, 08:175, 2019. arXiv:1905.03470, doi:10.1007/JHEP08(2019)175.
- [81] Jaroslav Adam et al. Measurement of jet quenching with semi-inclusive hadron-jet distributions in central Pb-Pb collisions at $\sqrt{s_{NN}} = 2.76$ TeV. *JHEP*, 09:170, 2015. arXiv:1506.03984, doi:10.1007/JHEP09(2015)170.
- [82] Georges Aad et al. Measurement of the jet radius and transverse momentum dependence of inclusive jet suppression in lead-lead collisions at $\sqrt{s_{NN}} = 2.76$ TeV with the ATLAS detector. *Phys. Lett. B*, 719:220–241, 2013. arXiv:1208.1967, doi:10.1016/j.physletb.2013.01.024.
- [83] L. Adamczyk et al. Measurements of jet quenching with semi-inclusive hadron+jet distributions in Au+Au collisions at $\sqrt{s_{NN}} = 200$ GeV. *Phys. Rev. C*, 96(2):024905, 2017. arXiv:1702.01108, doi:10.1103/PhysRevC.96.024905.

- [84] Rüdiger Haake and Constantin Loizides. Machine Learning based jet momentum reconstruction in heavy-ion collisions. *Phys. Rev. C*, 99(6):064904, 2019. [arXiv:1810.06324](#), [doi:10.1103/PhysRevC.99.064904](#).
- [85] Andrew J. Larkoski, Simone Marzani, Gregory Soyez, and Jesse Thaler. Soft Drop. *JHEP*, 05:146, 2014. [arXiv:1402.2657](#), [doi:10.1007/JHEP05\(2014\)146](#).
- [86] James Mulligan and Mateusz Ploskon. Identifying groomed jet splittings in heavy-ion collisions. *Phys. Rev. C*, 102(4):044913, 2020. [arXiv:2006.01812](#), [doi:10.1103/PhysRevC.102.044913](#).
- [87] G. D’Agostini. A Multidimensional unfolding method based on Bayes’ theorem. *Nucl. Instrum. Meth. A*, 362:487–498, 1995. [doi:10.1016/0168-9002\(95\)00274-X](#).
- [88] Andreas Hocker and Vakhtang Kartvelishvili. SVD approach to data unfolding. *Nucl. Instrum. Meth. A*, 372:469–481, 1996. [arXiv:hep-ph/9509307](#), [doi:10.1016/0168-9002\(95\)01478-0](#).
- [89] Stefan Schmitt. TUnfold: an algorithm for correcting migration effects in high energy physics. *JINST*, 7:T10003, 2012. [arXiv:1205.6201](#), [doi:10.1088/1748-0221/7/10/T10003](#).
- [90] Anders Andreassen, Patrick T. Komiske, Eric M. Metodiev, Benjamin Nachman, and Jesse Thaler. OmniFold: A Method to Simultaneously Unfold All Observables. *Phys. Rev. Lett.*, 124(18):182001, 2020. [arXiv:1911.09107](#), [doi:10.1103/PhysRevLett.124.182001](#).
- [91] Yuri L. Dokshitzer, G. D. Leder, S. Moretti, and B. R. Webber. Better jet clustering algorithms. *JHEP*, 08:001, 1997. [arXiv:hep-ph/9707323](#), [doi:10.1088/1126-6708/1997/08/001](#).
- [92] Stephen D. Ellis and Davison E. Soper. Successive combination jet algorithm for hadron collisions. *Phys. Rev. D*, 48:3160–3166, 1993. [arXiv:hep-ph/9305266](#), [doi:10.1103/PhysRevD.48.3160](#).
- [93] Frédéric A. Dreyer, Gavin P. Salam, and Grégory Soyez. The Lund Jet Plane. *JHEP*, 12:064, 2018. [arXiv:1807.04758](#), [doi:10.1007/JHEP12\(2018\)064](#).

- [94] Jonathan M. Butterworth, Adam R. Davison, Mathieu Rubin, and Gavin P. Salam. Jet substructure as a new Higgs search channel at the LHC. *Phys. Rev. Lett.*, 100:242001, 2008. [arXiv:0802.2470](#), [doi:10.1103/PhysRevLett.100.242001](#).
- [95] Yacine Mehtar-Tani, Alba Soto-Ontoso, and Konrad Tywoniuk. Dynamical grooming of QCD jets. *Phys. Rev. D*, 101(3):034004, 2020. [arXiv:1911.00375](#), [doi:10.1103/PhysRevD.101.034004](#).
- [96] David Krohn, Jesse Thaler, and Lian-Tao Wang. Jet Trimming. *JHEP*, 02:084, 2010. [arXiv:0912.1342](#), [doi:10.1007/JHEP02\(2010\)084](#).
- [97] Michael L. Miller, Klaus Reygers, Stephen J. Sanders, and Peter Steinberg. Glauber modeling in high energy nuclear collisions. *Ann. Rev. Nucl. Part. Sci.*, 57:205–243, 2007. [arXiv:nucl-ex/0701025](#), [doi:10.1146/annurev.nucl.57.090506.123020](#).
- [98] Andrew J. Larkoski, Jesse Thaler, and Wouter J. Waalewijn. Gaining (Mutual) Information about Quark/Gluon Discrimination. *JHEP*, 11:129, 2014. [arXiv:1408.3122](#), [doi:10.1007/JHEP11\(2014\)129](#).
- [99] Shreyasi Acharya et al. Measurements of inclusive jet spectra in pp and central Pb-Pb collisions at $\sqrt{s_{NN}} = 5.02$ TeV. *Phys. Rev. C*, 101(3):034911, 2020. [arXiv:1909.09718](#), [doi:10.1103/PhysRevC.101.034911](#).
- [100] Morad Aaboud et al. Measurement of the nuclear modification factor for inclusive jets in Pb+Pb collisions at $\sqrt{s_{NN}} = 5.02$ TeV with the ATLAS detector. *Phys. Lett. B*, 790:108–128, 2019. [arXiv:1805.05635](#), [doi:10.1016/j.physletb.2018.10.076](#).
- [101] J. Adam et al. Measurement of inclusive charged-particle jet production in Au + Au collisions at $\sqrt{s_{NN}} = 200$ GeV. *Phys. Rev. C*, 102(5):054913, 2020. [arXiv:2006.00582](#), [doi:10.1103/PhysRevC.102.054913](#).
- [102] B. Abelev et al. Measurement of charged jet suppression in Pb-Pb collisions at $\sqrt{s_{NN}} = 2.76$ TeV. *JHEP*, 03:013, 2014. [arXiv:1311.0633](#), [doi:10.1007/JHEP03\(2014\)013](#).
- [103] A. Adare et al. Neutral pion production with respect to centrality and reaction plane in Au+Au collisions at $\sqrt{s_{NN}}=200$ GeV. *Phys. Rev. C*, 87(3):034911, 2013. [arXiv:1208.2254](#), [doi:10.1103/PhysRevC.87.034911](#).

- [104] Scott Pratt, Evan Sangaline, Paul Sorensen, and Hui Wang. Constraining the Eq. of State of Super-Hadronic Matter from Heavy-Ion Collisions. *Phys. Rev. Lett.*, 114:202301, 2015. arXiv:1501.04042, doi:10.1103/PhysRevLett.114.202301.
- [105] Jonah E. Bernhard, J. Scott Moreland, and Steffen A. Bass. Bayesian estimation of the specific shear and bulk viscosity of quark–gluon plasma. *Nature Phys.*, 15(11):1113–1117, 2019. doi:10.1038/s41567-019-0611-8.
- [106] D. Everett et al. Multisystem Bayesian constraints on the transport coefficients of QCD matter. *Phys. Rev. C*, 103(5):054904, 2021. arXiv:2011.01430, doi:10.1103/PhysRevC.103.054904.
- [107] Govert Nijs, Wilke van der Schee, Umut Gürsoy, and Raimond Snellings. Bayesian analysis of heavy ion collisions with the heavy ion computational framework Trajectum. *Phys. Rev. C*, 103(5):054909, 2021. arXiv:2010.15134, doi:10.1103/PhysRevC.103.054909.
- [108] Yayun He, Long-Gang Pang, and Xin-Nian Wang. Bayesian extraction of jet energy loss distributions in heavy-ion collisions. *Phys. Rev. Lett.*, 122(25):252302, 2019. arXiv:1808.05310, doi:10.1103/PhysRevLett.122.252302.
- [109] Weiyao Ke and Xin-Nian Wang. QGP modification to single inclusive jets in a calibrated transport model. 10 2020. arXiv:2010.13680.
- [110] S. Cao et al. Determining the jet transport coefficient \hat{q} from inclusive hadron suppression measurements using Bayesian parameter estimation. 2 2021. arXiv:2102.11337.
- [111] A. Adare et al. Neutral pion production with respect to centrality and reaction plane in Au+Au collisions at $\sqrt{s_{NN}}=200$ GeV. *Phys. Rev. C*, 87(3):034911, 2013. arXiv:1208.2254, doi:10.1103/PhysRevC.87.034911.
- [112] A. Adare et al. An Upgrade Proposal from the PHENIX Collaboration. 1 2015. arXiv:1501.06197.
- [113] Thorsten Renk. Biased showers: A common conceptual framework for the interpretation of high- P_T observables in heavy-ion collisions. *Phys. Rev. C*, 88(5):054902, 2013. arXiv:1212.0646, doi:10.1103/PhysRevC.88.054902.

- [114] José Guilherme Milhano and Korinna Christine Zapp. Origins of the di-jet asymmetry in heavy ion collisions. *Eur. Phys. J. C*, 76(5):288, 2016. arXiv:1512.08107, doi:10.1140/epjc/s10052-016-4130-9.
- [115] Xin-Nian Wang, Miklos Gyulassy, and Michael Plumer. The LPM effect in QCD and radiative energy loss in a quark gluon plasma. *Phys. Rev. D*, 51:3436–3446, 1995. arXiv:hep-ph/9408344, doi:10.1103/PhysRevD.51.3436.
- [116] Paul M. Chesler, Kristan Jensen, Andreas Karch, and Laurence G. Yaffe. Light quark energy loss in strongly-coupled $N = 4$ supersymmetric Yang-Mills plasma. *Phys. Rev. D*, 79:125015, 2009. arXiv:0810.1985, doi:10.1103/PhysRevD.79.125015.
- [117] A. Adare et al. Azimuthal anisotropy of neutral pion production in Au+Au collisions at $\sqrt{(s_N N)} = 200$ GeV: Path-length dependence of jet quenching and the role of initial geometry. *Phys. Rev. Lett.*, 105:142301, 2010. arXiv:1006.3740, doi:10.1103/PhysRevLett.105.142301.
- [118] Jacquelyn Noronha-Hostler, Barbara Betz, Jorge Noronha, and Miklos Gyulassy. Event-by-event hydrodynamics + jet energy loss: A solution to the $R_{AA} \otimes v_2$ puzzle. *Phys. Rev. Lett.*, 116(25):252301, 2016. arXiv:1602.03788, doi:10.1103/PhysRevLett.116.252301.
- [119] Georges Aad et al. Measurement of the Azimuthal Angle Dependence of Inclusive Jet Yields in Pb+Pb Collisions at $\sqrt{s_{NN}} = 2.76$ TeV with the ATLAS detector. *Phys. Rev. Lett.*, 111(15):152301, 2013. arXiv:1306.6469, doi:10.1103/PhysRevLett.111.152301.
- [120] Jaroslav Adam et al. Azimuthal anisotropy of charged jet production in $\sqrt{s_{NN}} = 2.76$ TeV Pb-Pb collisions. *Phys. Lett. B*, 753:511–525, 2016. arXiv:1509.07334, doi:10.1016/j.physletb.2015.12.047.
- [121] Measurements of Jet Azimuthal Anisotropies in Pb+Pb collisions at $\sqrt{s_{NN}} = 5.02$ TeV. 6 2020.
- [122] A. M. Sirunyan et al. Azimuthal anisotropy of charged particles with transverse momentum up to 100 GeV/ c in PbPb collisions at $\sqrt{s_{NN}}=5.02$ TeV. *Phys. Lett. B*, 776:195–216, 2018. arXiv:1702.00630, doi:10.1016/j.physletb.2017.11.041.

- [123] Georges Aad et al. Transverse momentum and process dependent azimuthal anisotropies in $\sqrt{s_{NN}} = 8.16$ TeV p +Pb collisions with the ATLAS detector. *Eur. Phys. J. C*, 80(1):73, 2020. [arXiv:1910.13978](#), [doi:10.1140/epjc/s10052-020-7624-4](#).
- [124] Jaroslav Adam et al. Measurement of charged jet production cross sections and nuclear modification in p-Pb collisions at $\sqrt{s_{NN}} = 5.02$ TeV. *Phys. Lett. B*, 749:68–81, 2015. [arXiv:1503.00681](#), [doi:10.1016/j.physletb.2015.07.054](#).
- [125] Vardan Khachatryan et al. Charged-particle nuclear modification factors in PbPb and pPb collisions at $\sqrt{s_{NN}} = 5.02$ TeV. *JHEP*, 04:039, 2017. [arXiv:1611.01664](#), [doi:10.1007/JHEP04\(2017\)039](#).
- [126] Georges Aad et al. Observation of a Centrality-Dependent Dijet Asymmetry in Lead-Lead Collisions at $\sqrt{s_{NN}} = 2.77$ TeV with the ATLAS Detector at the LHC. *Phys. Rev. Lett.*, 105:252303, 2010. [arXiv:1011.6182](#), [doi:10.1103/PhysRevLett.105.252303](#).
- [127] Measurement of the dijet momentum balance in Pb+Pb and pp collisions at $\sqrt{s_{NN}} = 5.02$ TeV with the ATLAS detector. 6 2020.
- [128] Morad Aaboud et al. Measurement of jet p_T correlations in Pb+Pb and pp collisions at $\sqrt{s_{NN}} = 2.76$ TeV with the ATLAS detector. *Phys. Lett. B*, 774:379–402, 2017. [arXiv:1706.09363](#), [doi:10.1016/j.physletb.2017.09.078](#).
- [129] Morad Aaboud et al. Measurement of jet fragmentation in Pb+Pb and pp collisions at $\sqrt{s_{NN}} = 5.02$ TeV with the ATLAS detector. *Phys. Rev. C*, 98(2):024908, 2018. [arXiv:1805.05424](#), [doi:10.1103/PhysRevC.98.024908](#).
- [130] Martin Spousta and Brian Cole. Interpreting single jet measurements in Pb + Pb collisions at the LHC. *Eur. Phys. J. C*, 76(2):50, 2016. [arXiv:1504.05169](#), [doi:10.1140/epjc/s10052-016-3896-0](#).
- [131] Serguei Chatrchyan et al. Modification of Jet Shapes in PbPb Collisions at $\sqrt{s_{NN}} = 2.76$ TeV. *Phys. Lett. B*, 730:243–263, 2014. [arXiv:1310.0878](#), [doi:10.1016/j.physletb.2014.01.042](#).
- [132] Shreyasi Acharya et al. Medium modification of the shape of small-radius jets in central Pb-Pb collisions at $\sqrt{s_{NN}} = 2.76$ TeV. *JHEP*, 10:139, 2018. [arXiv:1807.06854](#), [doi:10.1007/JHEP10\(2018\)139](#).

- [133] Torbjörn Sjöstrand, Stefan Ask, Jesper R. Christiansen, Richard Corke, Nishita Desai, Philip Ilten, Stephen Mrenna, Stefan Prestel, Christine O. Rasmussen, and Peter Z. Skands. An introduction to PYTHIA 8.2. *Comput. Phys. Commun.*, 191:159–177, 2015. [arXiv:1410.3012](#), [doi:10.1016/j.cpc.2015.01.024](#).
- [134] Albert M Sirunyan et al. Measurement of quark- and gluon-like jet fractions using jet charge in PbPb and pp collisions at 5.02 TeV. *JHEP*, 07:115, 2020. [arXiv:2004.00602](#), [doi:10.1007/JHEP07\(2020\)115](#).
- [135] Albert M Sirunyan et al. Measurement of quark- and gluon-like jet fractions using jet charge in PbPb and pp collisions at 5.02 TeV. *JHEP*, 07:115, 2020. [arXiv:2004.00602](#), [doi:10.1007/JHEP07\(2020\)115](#).
- [136] Study of quark and gluon jet substructure in dijet and Z +jet events from pp collisions. 2021.
- [137] Morad Aaboud et al. Measurement of the inclusive jet cross-sections in proton-proton collisions at $\sqrt{s} = 8$ TeV with the ATLAS detector. *JHEP*, 09:020, 2017. [arXiv:1706.03192](#), [doi:10.1007/JHEP09\(2017\)020](#).
- [138] Serguei Chatrchyan et al. Studies of jet quenching using isolated-photon+jet correlations in PbPb and pp collisions at $\sqrt{s_{NN}} = 2.76$ TeV. *Phys. Lett. B*, 718:773–794, 2013. [arXiv:1205.0206](#), [doi:10.1016/j.physletb.2012.11.003](#).
- [139] Albert M Sirunyan et al. Study of jet quenching with isolated-photon+jet correlations in PbPb and pp collisions at $\sqrt{s_{NN}} = 5.02$ TeV. *Phys. Lett. B*, 785:14–39, 2018. [arXiv:1711.09738](#), [doi:10.1016/j.physletb.2018.07.061](#).
- [140] Morad Aaboud et al. Measurement of photon–jet transverse momentum correlations in 5.02 TeV Pb + Pb and pp collisions with ATLAS. *Phys. Lett. B*, 789:167–190, 2019. [arXiv:1809.07280](#), [doi:10.1016/j.physletb.2018.12.023](#).
- [141] Albert M Sirunyan et al. Study of Jet Quenching with $Z + jet$ Correlations in Pb-Pb and pp Collisions at $\sqrt{s_{NN}} = 5.02$ TeV. *Phys. Rev. Lett.*, 119(8):082301, 2017. [arXiv:1702.01060](#), [doi:10.1103/PhysRevLett.119.082301](#).
- [142] Albert M Sirunyan et al. Observation of Medium-Induced Modifications of Jet Fragmentation in Pb-Pb Collisions at $\sqrt{s_{NN}} = 5.02$ TeV Using Isolated

- Photon-Tagged Jets. *Phys. Rev. Lett.*, 121(24):242301, 2018. [arXiv:1801.04895](#), [doi:10.1103/PhysRevLett.121.242301](#).
- [143] Morad Aaboud et al. Comparison of Fragmentation Functions for Jets Dominated by Light Quarks and Gluons from pp and Pb+Pb Collisions in ATLAS. *Phys. Rev. Lett.*, 123(4):042001, 2019. [arXiv:1902.10007](#), [doi:10.1103/PhysRevLett.123.042001](#).
- [144] A. Adare et al. Medium modification of jet fragmentation in Au + Au collisions at $\sqrt{s_{NN}} = 200$ GeV measured in direct photon-hadron correlations. *Phys. Rev. Lett.*, 111(3):032301, 2013. [arXiv:1212.3323](#), [doi:10.1103/PhysRevLett.111.032301](#).
- [145] B. I. Abelev et al. Studying Parton Energy Loss in Heavy-Ion Collisions via Direct-Photon and Charged-Particle Azimuthal Correlations. *Phys. Rev. C*, 82:034909, 2010. [arXiv:0912.1871](#), [doi:10.1103/PhysRevC.82.034909](#).
- [146] Huijun Ge. PHENIX results on direct photon-hadron correlations. *Nucl. Part. Phys. Proc.*, 289-290:313-316, 2017. [arXiv:1703.09374](#), [doi:10.1016/j.nuclphysbps.2017.05.072](#).
- [147] Morad Aaboud et al. Measurement of jet fragmentation in Pb+Pb and pp collisions at $\sqrt{s_{NN}} = 2.76$ TeV with the ATLAS detector at the LHC. *Eur. Phys. J. C*, 77(6):379, 2017. [arXiv:1702.00674](#), [doi:10.1140/epjc/s10052-017-4915-5](#).
- [148] Yuri L. Dokshitzer, Valery A. Khoze, and S. I. Troian. On specific QCD properties of heavy quark fragmentation ('dead cone'). *J. Phys. G*, 17:1602-1604, 1991. [doi:10.1088/0954-3899/17/10/023](#).
- [149] Nestor Armesto, Carlos A. Salgado, and Urs Achim Wiedemann. Medium induced gluon radiation off massive quarks fills the dead cone. *Phys. Rev. D*, 69:114003, 2004. [arXiv:hep-ph/0312106](#), [doi:10.1103/PhysRevD.69.114003](#).
- [150] Serguei Chatrchyan et al. Evidence of b-Jet Quenching in PbPb Collisions at $\sqrt{s_{NN}} = 2.76$ TeV. *Phys. Rev. Lett.*, 113(13):132301, 2014. [Erratum: *Phys.Rev.Lett.* 115, 029903 (2015)]. [arXiv:1312.4198](#), [doi:10.1103/PhysRevLett.113.132301](#).

- [151] Albert M Sirunyan et al. Comparing transverse momentum balance of b jet pairs in pp and PbPb collisions at $\sqrt{s_{\text{NN}}} = 5.02$ TeV. *JHEP*, 03:181, 2018. [arXiv:1802.00707](#), [doi:10.1007/JHEP03\(2018\)181](#).
- [152] Shreyasi Acharya et al. Direct observation of the dead-cone effect in QCD. 6 2021. [arXiv:2106.05713](#).
- [153] Philip Ilten, Nicholas L. Rodd, Jesse Thaler, and Mike Williams. Disentangling Heavy Flavor at Colliders. *Phys. Rev. D*, 96(5):054019, 2017. [arXiv:1702.02947](#), [doi:10.1103/PhysRevD.96.054019](#).
- [154] Z. Citron et al. Report from Working Group 5: Future physics opportunities for high-density QCD at the LHC with heavy-ion and proton beams. *CERN Yellow Rep. Monogr.*, 7:1159–1410, 2019. [arXiv:1812.06772](#), [doi:10.23731/CYRM-2019-007.1159](#).
- [155] A. Adare et al. An Upgrade Proposal from the PHENIX Collaboration. 1 2015. [arXiv:1501.06197](#).
- [156] Andrew Larkoski, Simone Marzani, Jesse Thaler, Aashish Tripathy, and Wei Xue. Exposing the QCD Splitting Function with CMS Open Data. *Phys. Rev. Lett.*, 119(13):132003, 2017. [arXiv:1704.05066](#), [doi:10.1103/PhysRevLett.119.132003](#).
- [157] Albert M Sirunyan et al. Measurement of the Splitting Function in pp and Pb-Pb Collisions at $\sqrt{s_{\text{NN}}} = 5.02$ TeV. *Phys. Rev. Lett.*, 120(14):142302, 2018. [arXiv:1708.09429](#), [doi:10.1103/PhysRevLett.120.142302](#).
- [158] Shreyasi Acharya et al. Exploration of jet substructure using iterative declustering in pp and Pb–Pb collisions at LHC energies. *Phys. Lett. B*, 802:135227, 2020. [arXiv:1905.02512](#), [doi:10.1016/j.physletb.2020.135227](#).
- [159] Shreyasi Acharya et al. Measurement of the groomed jet radius and momentum splitting fraction in pp and Pb–Pb collisions at $\sqrt{s_{\text{NN}}} = 5.02$ TeV. 7 2021. [arXiv:2107.12984](#).
- [160] Kolja Kauder. JETSCAPE v1.0 Quickstart Guide. *Nucl. Phys. A*, 982:615–618, 2019. [arXiv:1807.09615](#), [doi:10.1016/j.nuclphysa.2018.09.033](#).
- [161] Yi-Lun Du, Daniel Pablos, and Konrad Tywoniuk. Jet tomography in heavy ion collisions with deep learning. 6 2. [arXiv:2106.11271](#).

- [162] P. Caucal, E. Iancu, A. H. Mueller, and G. Soyez. Vacuum-like jet fragmentation in a dense QCD medium. *Phys. Rev. Lett.*, 120:232001, 2018. [arXiv:1801.09703](#), [doi:10.1103/PhysRevLett.120.232001](#).
- [163] Jesse Thaler and Ken Van Tilburg. Identifying Boosted Objects with N-subjettiness. *JHEP*, 03:015, 2011. [arXiv:1011.2268](#), [doi:10.1007/JHEP03\(2011\)015](#).
- [164] Shreyasi Acharya et al. First measurements of N-subjettiness in central Pb–Pb collisions at $\sqrt{s_{\text{NN}}} = 2.76$ TeV. 5 2021. [arXiv:2105.04936](#).
- [165] Measurement of suppression of large-radius jets and its dependence on substructure in Pb+Pb at 5.02 TeV by ATLAS detector. 11 2019.
- [166] Torbjorn Sjostrand, Stephen Mrenna, and Peter Z. Skands. A Brief Introduction to PYTHIA 8.1. *Comput. Phys. Commun.*, 178:852–867, 2008. [doi:10.1016/j.cpc.2008.01.036](#).
- [167] A. M. Sirunyan et al. Measurement of jet substructure observables in $t\bar{t}$ events from proton-proton collisions at $\sqrt{s} = 13$ TeV. *Phys. Rev. D*, 98(9):092014, 2018. [arXiv:1808.07340](#), [doi:10.1103/PhysRevD.98.092014](#).
- [168] Daniel Pablos. Jet Suppression From a Small to Intermediate to Large Radius. *Phys. Rev. Lett.*, 124(5):052301, 2020. [arXiv:1907.12301](#), [doi:10.1103/PhysRevLett.124.052301](#).
- [169] Jaroslav Adam et al. Measurement of jet quenching with semi-inclusive hadron-jet distributions in central Pb-Pb collisions at $\sqrt{s_{\text{NN}}} = 2.76$ TeV. *JHEP*, 09:170, 2015. [arXiv:1506.03984](#), [doi:10.1007/JHEP09\(2015\)170](#).
- [170] Morad Aaboud et al. Measurement of the nuclear modification factor for inclusive jets in Pb+Pb collisions at $\sqrt{s_{\text{NN}}} = 5.02$ TeV with the ATLAS detector. *Phys. Lett. B*, 790:108–128, 2019. [arXiv:1805.05635](#), [doi:10.1016/j.physletb.2018.10.076](#).
- [171] S. Acharya et al. First measurement of jet mass in Pb–Pb and p–Pb collisions at the LHC. *Phys. Lett. B*, 776:249–264, 2018. [arXiv:1702.00804](#), [doi:10.1016/j.physletb.2017.11.044](#).
- [172] Raghav Kunnawalkam Elayavalli and Korinna Christine Zapp. Medium response in JEWEL and its impact on jet shape observables in heavy ion collisions. *JHEP*, 07:141, 2017. [arXiv:1707.01539](#), [doi:10.1007/JHEP07\(2017\)141](#).

- [173] Albert M Sirunyan et al. First measurement of large area jet transverse momentum spectra in heavy-ion collisions. *JHEP*, 05:284, 2021. [arXiv:2102.13080](#), [doi:10.1007/JHEP05\(2021\)284](#).
- [174] Georges Aad et al. Measurement of angular and momentum distributions of charged particles within and around jets in Pb+Pb and *pp* collisions at $\sqrt{s_{NN}} = 5.02$ TeV with the ATLAS detector. *Phys. Rev. C*, 100(6):064901, 2019. [Erratum: *Phys.Rev.C* 101, 059903 (2020)]. [arXiv:1908.05264](#), [doi:10.1103/PhysRevC.100.064901](#).
- [175] Vardan Khachatryan et al. Correlations between jets and charged particles in PbPb and *pp* collisions at $\sqrt{s_{NN}} = 2.76$ TeV. *JHEP*, 02:156, 2016. [arXiv:1601.00079](#), [doi:10.1007/JHEP02\(2016\)156](#).
- [176] Vardan Khachatryan et al. Decomposing transverse momentum balance contributions for quenched jets in PbPb collisions at $\sqrt{s_{NN}} = 2.76$ TeV. *JHEP*, 11:055, 2016. [arXiv:1609.02466](#), [doi:10.1007/JHEP11\(2016\)055](#).
- [177] Albert M Sirunyan et al. Jet properties in PbPb and *pp* collisions at $\sqrt{s_{NN}} = 5.02$ TeV. *JHEP*, 05:006, 2018. [arXiv:1803.00042](#), [doi:10.1007/JHEP05\(2018\)006](#).
- [178] Albert M Sirunyan et al. In-medium modification of dijets in PbPb collisions at $\sqrt{s_{NN}} = 5.02$ TeV. 1 2021. [arXiv:2101.04720](#).
- [179] Georges Aad et al. Medium-Induced Modification of *Z*-Tagged Charged Particle Yields in *Pb + Pb* Collisions at 5.02 TeV with the ATLAS Detector. *Phys. Rev. Lett.*, 126(7):072301, 2021. [arXiv:2008.09811](#), [doi:10.1103/PhysRevLett.126.072301](#).
- [180] Francesco D’Eramo, Mindaugas Lekaveckas, Hong Liu, and Krishna Rajagopal. Momentum Broadening in Weakly Coupled Quark-Gluon Plasma (with a view to finding the quasiparticles within liquid quark-gluon plasma). *JHEP*, 05:031, 2013. [arXiv:1211.1922](#), [doi:10.1007/JHEP05\(2013\)031](#).
- [181] Yacine Mehtar-Tani, Alba Soto-Ontoso, and Konrad Tywoniuk. Tagging boosted hadronic objects with dynamical grooming. *Phys. Rev. D*, 102:114013, 2020. [arXiv:2005.07584](#), [doi:10.1103/PhysRevD.102.114013](#).
- [182] Georges Aad et al. Observation of a Centrality-Dependent Dijet Asymmetry in Lead-Lead Collisions at $\sqrt{s_{NN}} = 2.77$ TeV with the ATLAS Detector at the

- LHC. *Phys. Rev. Lett.*, 105:252303, 2010. [arXiv:1011.6182](#), [doi:10.1103/PhysRevLett.105.252303](#).
- [183] Albert M Sirunyan et al. Study of jet quenching with isolated-photon+jet correlations in PbPb and pp collisions at $\sqrt{s_{NN}} = 5.02$ TeV. *Phys. Lett. B*, 785:14–39, 2018. [arXiv:1711.09738](#), [doi:10.1016/j.physletb.2018.07.061](#).
- [184] A. H. Mueller, Bin Wu, Bo-Wen Xiao, and Feng Yuan. Probing Transverse Momentum Broadening in Heavy Ion Collisions. *Phys. Lett. B*, 763:208–212, 2016. [arXiv:1604.04250](#), [doi:10.1016/j.physletb.2016.10.037](#).
- [185] James L. Nagle and William A. Zajc. Small System Collectivity in Relativistic Hadronic and Nuclear Collisions. *Ann. Rev. Nucl. Part. Sci.*, 68:211–235, 2018. [arXiv:1801.03477](#), [doi:10.1146/annurev-nucl-101916-123209](#).
- [186] A. Adare et al. Centrality-dependent modification of jet-production rates in deuteron-gold collisions at $\sqrt{s_{NN}}=200$ GeV. *Phys. Rev. Lett.*, 116(12):122301, 2016. [arXiv:1509.04657](#), [doi:10.1103/PhysRevLett.116.122301](#).
- [187] Georges Aad et al. Centrality and rapidity dependence of inclusive jet production in $\sqrt{s_{NN}} = 5.02$ TeV proton-lead collisions with the ATLAS detector. *Phys. Lett. B*, 748:392–413, 2015. [arXiv:1412.4092](#), [doi:10.1016/j.physletb.2015.07.023](#).
- [188] J. Adams et al. Evidence from d + Au measurements for final state suppression of high p(T) hadrons in Au+Au collisions at RHIC. *Phys. Rev. Lett.*, 91:072304, 2003. [arXiv:nucl-ex/0306024](#), [doi:10.1103/PhysRevLett.91.072304](#).
- [189] S. S. Adler et al. Absence of suppression in particle production at large transverse momentum in $S(NN)^{1/2} = 200$ -GeV d + Au collisions. *Phys. Rev. Lett.*, 91:072303, 2003. [arXiv:nucl-ex/0306021](#), [doi:10.1103/PhysRevLett.91.072303](#).
- [190] Shreyasi Acharya et al. Constraints on jet quenching in p-Pb collisions at $\sqrt{s_{NN}} = 5.02$ TeV measured by the event-activity dependence of semi-inclusive hadron-jet distributions. *Phys. Lett. B*, 783:95–113, 2018. [arXiv:1712.05603](#), [doi:10.1016/j.physletb.2018.05.059](#).
- [191] Morad Aaboud et al. Measurement of jet fragmentation in 5.02 TeV proton-lead and proton-proton collisions with the ATLAS detector. *Nucl. Phys. A*, 978:65, 2018. [arXiv:1706.02859](#), [doi:10.1016/j.nuclphysa.2018.07.006](#).

- [192] Serguei Chatrchyan et al. Studies of dijet transverse momentum balance and pseudorapidity distributions in pPb collisions at $\sqrt{s_{\text{NN}}} = 5.02$ TeV. *Eur. Phys. J. C*, 74(7):2951, 2014. [arXiv:1401.4433](#), [doi:10.1140/epjc/s10052-014-2951-y](#).
- [193] Shreyasi Acharya et al. Transverse momentum spectra and nuclear modification factors of charged particles in Xe-Xe collisions at $\sqrt{s_{\text{NN}}} = 5.44$ TeV. *Phys. Lett. B*, 788:166–179, 2019. [arXiv:1805.04399](#), [doi:10.1016/j.physletb.2018.10.052](#).
- [194] Alexander Huss, Aleksi Kurkela, Aleksas Mazeliauskas, Risto Paatelainen, Wilke van der Schee, and Urs Achim Wiedemann. Discovering Partonic Rescattering in Light Nucleus Collisions. *Phys. Rev. Lett.*, 126(19):192301, 2021. [arXiv:2007.13754](#), [doi:10.1103/PhysRevLett.126.192301](#).
- [195] Jasmine Brewer, Aleksas Mazeliauskas, and Wilke van der Schee. Opportunities of OO and pO collisions at the LHC. In *Opportunities of OO and pO collisions at the LHC*, 3 2021. [arXiv:2103.01939](#).
- [196] ALICE physics projections for a short oxygen-beam run at the LHC. May 2021. URL: <https://cds.cern.ch/record/2765973>.
- [197] Alexander Huss, Aleksi Kurkela, Aleksas Mazeliauskas, Risto Paatelainen, Wilke van der Schee, and Urs Achim Wiedemann. Predicting parton energy loss in small collision systems. *Phys. Rev. C*, 103(5):054903, 2021. [arXiv:2007.13758](#), [doi:10.1103/PhysRevC.103.054903](#).